

**NERC**

NORTH AMERICAN ELECTRIC  
RELIABILITY CORPORATION

# Application Guide

Computing Geomagnetically-Induced Current in  
the Bulk-Power System

December 2013

**RELIABILITY | ACCOUNTABILITY**



3353 Peachtree Road NE  
Suite 600, North Tower  
Atlanta, GA 30326

# Table of Contents

---

Table of Contents .....	ii
Preface.....	iii
Introduction.....	1
Organization.....	1
Overview .....	2
Chapter 1 – Geoelectric Field Calculations.....	4
Theory.....	5
Practical Details.....	7
Example Calculation.....	9
Chapter 2 – Modeling GIC .....	15
Theory .....	15
Time Series Calculations.....	17
Practical Details.....	18
Introduction .....	18
Transformers.....	20
Substation Ground Grid and Neutral Connected GIC Blocking Devices.....	23
Transmission Line Models.....	24
Blocking GIC in a Line .....	25
Shunt Devices.....	25
Chapter 3 – Modeling Refinements.....	26
Non-Uniform Source Fields.....	26
Non-Uniform Earth Structure .....	28
Including Neighboring Systems.....	28
References.....	30
Appendix I – Calculating Distance Between Substations .....	32
Appendix II – Example of GIC Calculations.....	35
Appendix III – NERC GMD Task Force Leadership Roster.....	39

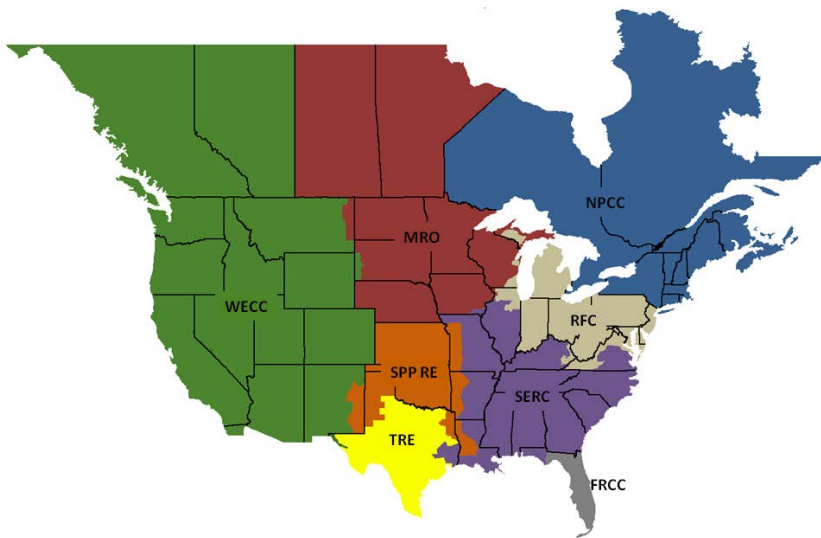
# Preface

---

The North American Electric Reliability Corporation (NERC) is a not-for-profit international regulatory authority whose mission is to ensure the reliability of the Bulk-Power System (BPS) in North America. NERC develops and enforces Reliability Standards; annually assesses seasonal and long-term reliability; monitors the BPS through system awareness; and educates, trains, and certifies industry personnel. NERC’s area of responsibility spans the continental United States, Canada, and the northern portion of Baja California, Mexico. NERC is the electric reliability organization (ERO) for North America, subject to oversight by the Federal Energy Regulatory Commission (FERC) and governmental authorities in Canada. NERC’s jurisdiction includes users, owners, and operators of the BPS, which serves more than 334 million people.

The North American BPS is divided into several assessment areas within the eight Regional Entity (RE) boundaries, as shown in the map and corresponding table below.

<b>FRCC</b>	Florida Reliability Coordinating Council
<b>MRO</b>	Midwest Reliability Organization
<b>NPCC</b>	Northeast Power Coordinating Council
<b>RFC</b>	Reliability <i>First</i> Corporation
<b>SERC</b>	SERC Reliability Corporation
<b>SPP-RE</b>	Southwest Power Pool Regional Entity
<b>TRE</b>	Texas Reliability Entity
<b>WECC</b>	Western Electric Coordinating Council



# Introduction

---

During geomagnetic disturbances, variations in the geomagnetic field induce quasi-dc voltages in the network which drive geomagnetically-induced currents (GIC) along transmission lines and through transformer windings to ground wherever there is a path for them to flow. The flow of these quasi-dc currents in transformer windings causes half-cycle saturation of transformer cores which leads to increased transformer hotspot heating, harmonic generation, and reactive power absorption – each of which can affect system reliability. As part of the assessment of geomagnetic disturbances (GMDs) impacts on the Bulk-Power System, it is necessary to model the GIC produced by different levels of geomagnetic activity. This guide presents theory and practical details for GIC modeling which can be used to explain the inner workings of commercially-available GIC modeling software packages or for setting up a GIC calculation procedure.

## Organization

The Geomagnetic Disturbance Task Force has produced four documents to provide practical information and guidance in the assessment of the effects of GMD on the Bulk-Power System. While interrelated, these documents each serve a distinct purpose and can be followed on a standalone basis.

### Geomagnetic Disturbance Planning Guide

This document provides guidance on how to carry out system assessment studies taking the effects of GMD into account. It describes the types of studies which should be performed, challenges in implementing each study type, and identifies the analytical tools and data resources required in each case.

### Transformer Modeling Guide

This guide summarizes the transformer models that are available for GMD planning studies. These fall into two categories: magnetic models that describe transformer var absorption and harmonic generation caused by GIC and thermal models that account for hot spot heating also caused by GIC. In the absence of detailed models or measurements carried out by transformer manufacturers, the guide summarizes “generic” values (and the inherent limitations thereof) for use in GMD studies.

### Application Guide for Computing Geomagnetically-Induced Current (GIC) in the Bulk-Power System

This reference document explains the theoretical background behind calculating geomagnetically-induced currents (GIC). A summary of underlying assumptions and techniques used in modern GMD simulation tools as well as data considerations is provided.

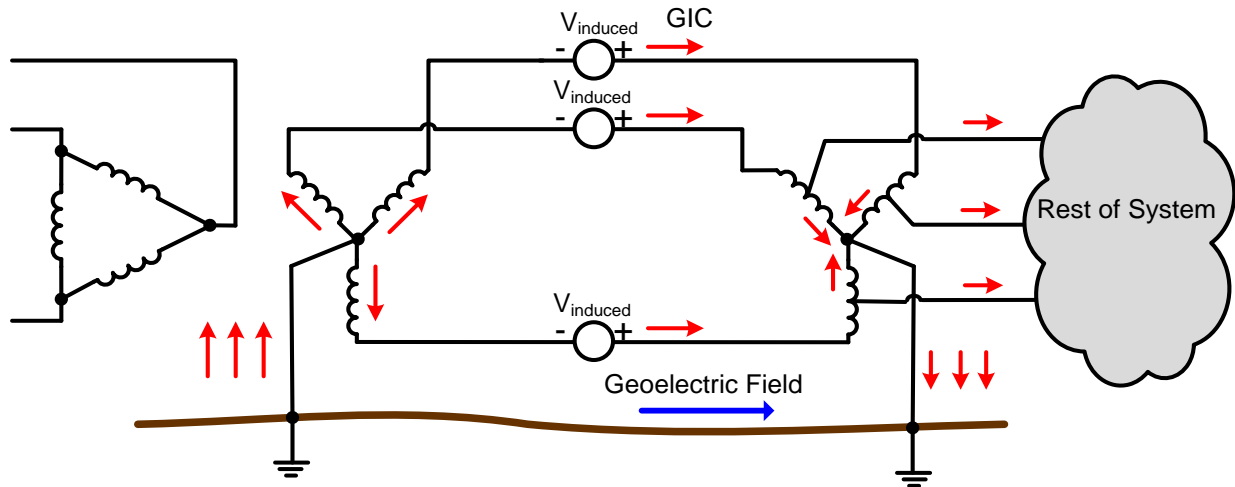
### Operating Procedure Template

This document provides guidance on the operating procedures that can be used in the management of a GMD event. The document supports the development of tailored operating procedures once studies have been conducted to assess the effects of GMD on the system.

## Overview

An example of the geomagnetic field induction process in a simplified network is depicted in Figure 1.

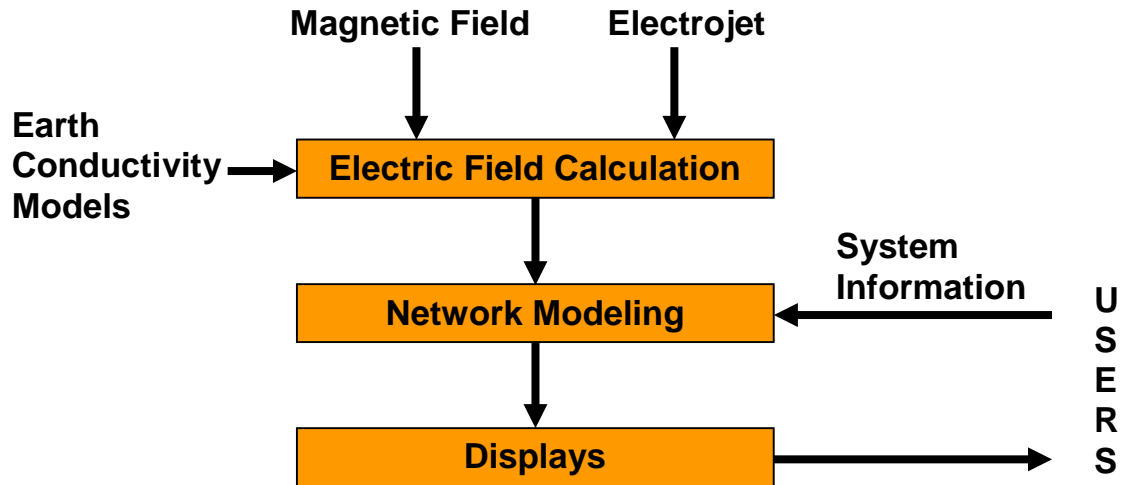
**Figure 1: GIC flow in a simplified power system**



GIC are considered quasi-dc relative to the power system frequency because of their low frequency (0.0001Hz to 1 Hz); thus, from a power system modeling perspective GIC can be considered as dc. The flow of these quasi-dc currents in transformer windings causes half-cycle saturation of transformer cores which leads to increased transformer hotspot heating, harmonic generation, and reactive power absorption – each of which can affect system reliability. As part of the assessment of geomagnetic disturbances (GMDs) impacts on bulk power systems, it is necessary to model the GIC produced by different levels of geomagnetic activity.

The process for computing GIC in a bulk power system comprises two steps (see

Figure 2). First, the geoelectric field must be estimated or directly determined from available geomagnetic data and earth conductivity models. When performing steady-state GIC calculations, the geoelectric field can be estimated from general tables which take into account both geomagnetic latitude and earth conductivity. Secondly, GIC flows are computed using circuit analysis techniques with a dc model of the bulk power system. Once the GIC flows are determined they are used as input data to other system studies such as power flow analysis and thermal analysis of transformers.

**Figure 2: Steps involved in calculating time series GIC in a power system**

The following sections present the theory and practical details for the electric field calculations and the GIC modeling. Modeling refinements to source fields and earth conductivity structures are discussed in later sections.

Several open source and commercially available modeling software packages have included many of the GIC calculations procedures described herein. Therefore, this guide can be used as an explanation of the internal working of these software packages or as guidance for setting up a calculation procedure.

# Chapter 1 – Geoelectric Field Calculations

---

GIC modeling uses geoelectric field values as input. When examining the GIC flow patterns across a network, it can be useful to perform steady state GIC calculations based on an assumed magnitude and direction of the geoelectric field. This approach is explained in the next section. However, determination of the GIC which occur over time during an actual geomagnetic disturbance requires the calculation of a time series geoelectric fields produced in response the geomagnetic field variations. The theory and procedures for performing these calculations are the topics of this section.

The geomagnetic field variations experienced by power systems at the earth's surface originate from electric currents flowing in the ionosphere or magnetosphere at heights of 100 km or greater. Compared to the heights of these source currents, the height of the transmission lines is insignificant and the electric field at the height of the transmission line can be assumed to be the same as the electric field at the earth's surface.

The magnetic field variations induce electric currents in the earth which also produce magnetic fields that contribute to the magnetic disturbances observed at the earth's surface. Inside the earth, the induced currents act to cancel external magnetic field variations leading to a decrease of the currents and fields with depth. At low frequencies, the skin depth  $\delta$  is characterized by

$$\delta = \sqrt{\frac{2}{\omega\mu\sigma}} \quad (1)$$

and is dependent upon: the angular frequency,  $\omega$ , in radians; the conductivity,  $\sigma$ , in S/m; and the free space value for the magnetic permeability  $\mu_0 = 4\pi \times 10^{-7}$  H/m [1].

Given the range of frequencies relevant to GIC (0.0001Hz to 1 Hz) and the conductivity values within the earth, magnetic field variations can penetrate hundreds of kilometers below the surface. Thus, the conductivity down through the earth's crust and into the mantle must be taken into account when determining the electric field at the surface. Additionally, the geoelectric field calculations must take into account the frequency-dependent behavior of the earth response. One method of accounting for frequency dependence is to decompose the magnetic field variations into their frequency components, calculate the earth response (surface impedance) at each frequency, and then combine these frequency components to give the electric field variation with time.

## Theory

The relationship between the geomagnetic field, earth surface impedance and the geoelectric field is described in (2) and (3)

$$E_x(\omega) = Z(\omega)H_y(\omega) \tag{2}$$

$$E_y(\omega) = -Z(\omega)H_x(\omega) \tag{3}$$

where  $E_x(\omega)$  is the Northward geoelectric field (V/m),  $E_y(\omega)$  is the Eastward geoelectric field (V/m),  $H_x(\omega)$  is the Northward geomagnetic field intensity (A/m),  $H_y(\omega)$  is the Eastward geomagnetic field intensity (A/m), and  $Z(\omega)$  is the earth surface impedance ( $\Omega$ ) [2].

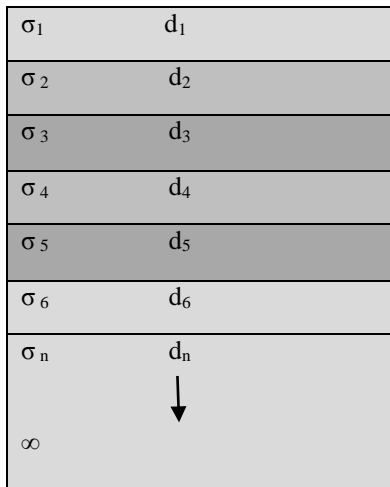
The relationship between the geomagnetic field intensity,  $H(\omega)$ , and the geomagnetic field density,  $B(\omega)$ , is given by,

$$B(\omega) = -\mu_0 H(\omega) \tag{4}$$

where,  $\mu_0$  is the magnetic permeability of free space.

The surface impedance,  $Z(\omega)$ , depends on the earth conductivity structure below the power system. The variation of conductivity with depth can be represented using a 1-D layered, laterally uniform earth model as depicted in Figure 3. A one-dimensional, or 1-D, model ignores lateral variations in conductivity but provides a reasonable approximation in many situations. However, near a conductivity boundary such as a coastline, a 2-D or 3-D earth model may provide more accurate results. 2-D and 3-D modeling considerations are discussed in later chapters.

**Figure 3: 1-D layered earth conductivity model**



The impedance at the surface of the earth can be calculated using recursive relations in a manner analogous to transmission line theory. Each layer is characterized by its propagation constant

$$k_n = \sqrt{j\omega\mu_0\sigma_n} \tag{5}$$



where,  $\omega$  is the angular frequency (rad/sec),  $\mu_0$  is the magnetic permeability of free space,  $\sigma_n$  is the conductivity of layer  $n$  ( $(\Omega\text{-m})^{-1}$ ), and  $r_n$  is the thickness of layer  $n$  (m).

For the bottom layer where there are no reflections, the impedance at the surface is

$$Z_n = \frac{j\omega\mu_0}{k_n} \tag{6}$$

Equation 7 is used to calculate the reflection coefficient seen by the layer above

$$r_n = \frac{1 - k_n \frac{Z_{n+1}}{j \cdot \omega \cdot \mu_0}}{1 + k_n \frac{Z_{n+1}}{j \cdot \omega \cdot \mu_0}} \tag{7}$$

which can then be used to calculate the impedance at the top surface of that layer

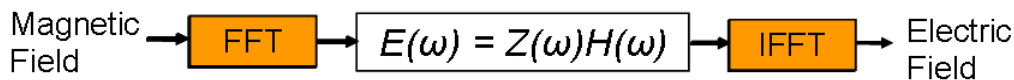
$$Z_n = j \cdot \omega \cdot \mu_0 \left( \frac{1 - r_n \cdot e^{-2k_n d_n}}{k_n (1 + r_n \cdot e^{-2k_n d_n})} \right) \tag{8}$$

These steps are then repeated for each layer up to the earth's surface [3].

The propagation constants and corresponding impedances are functions of frequency, thus, the sequence of calculations has to be repeated at each frequency. The exact frequencies needed to calculate the electric fields depend on the sampling rate of the magnetic data and the duration of the data used. The final set of surface impedance values represent the transfer function of the earth relating the electric and magnetic fields which will be used in the calculations of the geoelectric fields.

Frequency domain techniques are commonly employed to compute the geoelectric field. The sequence of operations for calculating geoelectric fields in this manner is shown in Figure 4. Starting with a time series of magnetic field values, i.e.  $B(t)$ , a Fast Fourier Transform (FFT) is used to obtain the frequency spectrum (magnitude and phase) of the magnetic field variations,  $B(\omega)$ . The magnetic field spectral value at each frequency is then multiplied by the corresponding surface impedance value (and divided by  $\mu_0$ ) to obtain the geoelectric field spectral value,  $E(\omega)$ . This then gives the frequency spectrum of the geoelectric field. An inverse Fast Fourier Transform (IFFT) is then used to obtain the geoelectric field values in the time domain,  $E(t)$ .

**Figure 4: Using magnetic data to calculate geoelectric fields.**



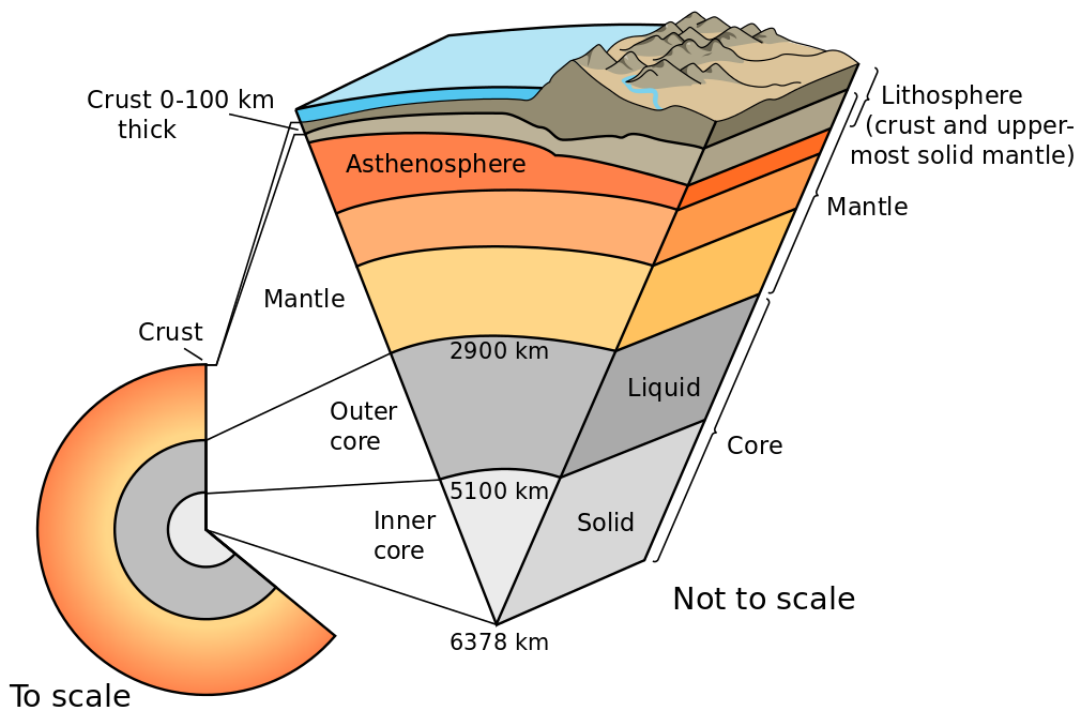
Time domain methods, such as the one presented in [4] and [5], can also be used to compute the geoelectric field as the two methods are numerically equivalent.

## Practical Details

Using the previously described 1-D modeling technique to represent the frequency-dependent behavior of the earth requires suitable values for the thicknesses and conductivities of the various layers. Skin depths, at the frequencies of concern in GIC studies, are kilometers or greater so only the average conductivities over depths on these scales need to be considered. Magnetic field variations pass through thin surface layers unaffected; therefore, the conductivities of surface soil layers are unimportant. Consequently, 'earth resistivity' values commonly used in fundamental frequency calculations (i.e., 60Hz) are not appropriate for GIC studies. Instead earth models have to be specially constructed.

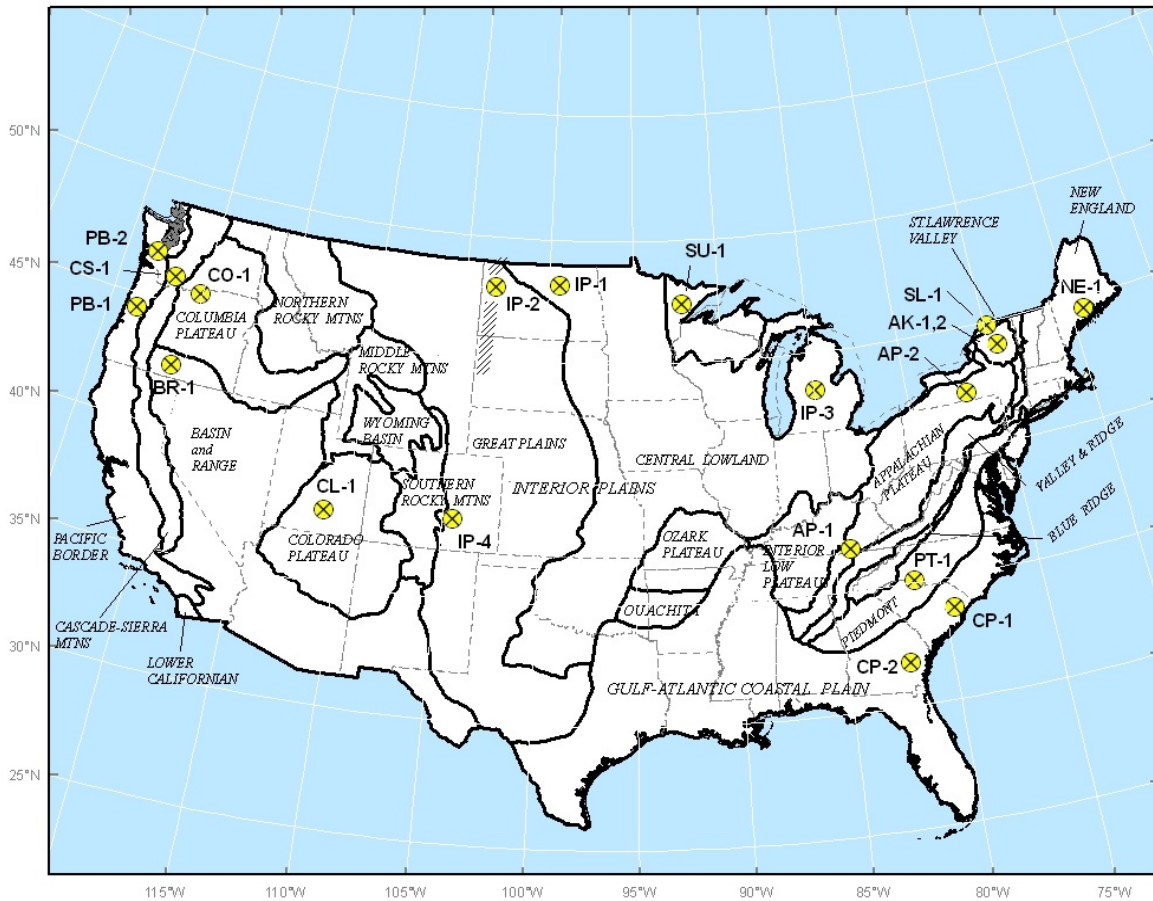
The conductivity of surface layers of the earth depends on the rock type: ranging from very resistive igneous rocks to more conductive sedimentary rocks. Below the surface layers, the earth consists of the crust, which is resistive, and below the crust is the mantle where increased pressures and temperatures lead to higher conductivities, as illustrated in Figure 5.

**Figure 5: Schematic of the internal structure of the Earth**



For a specific region, an earth conductivity model can be assembled from the results of magnetotelluric studies and geological information. Such earth conductivity models for various physiographic regions of North America are available from the United States Geological Survey (USGS - <http://geomag.usgs.gov/conductivity>) and the Geological Survey of Canada (GSC). Model locations and physiographic regions for the United States are shown in Figure 6. It is important to note that these models are preliminary and are expected to change with further assessments and validation. As such, caution is required when selecting and applying these models.

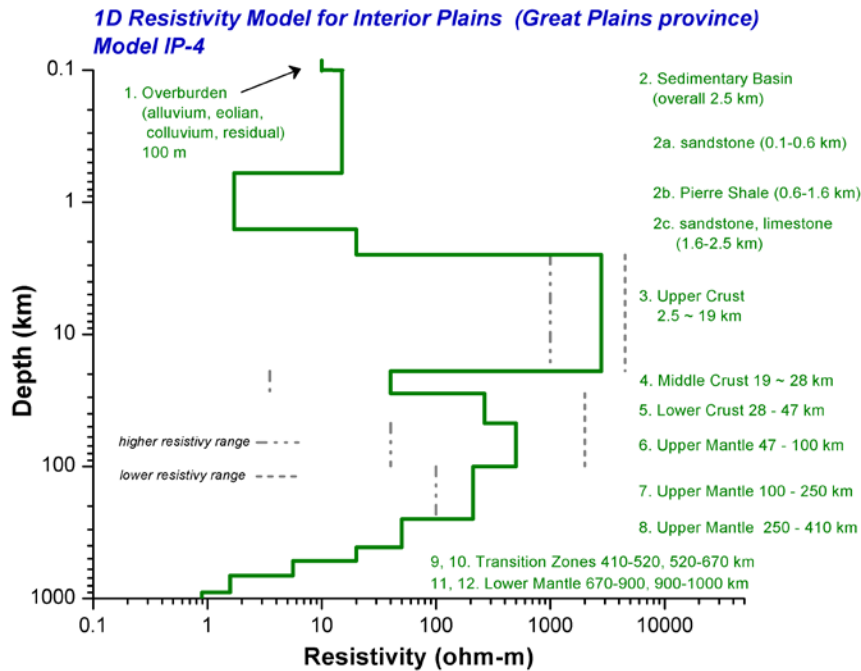
**Figure 6: Location of 1-D earth resistivity models with respect to physiographic regions of the contiguous United States [6].**



## Example Calculation

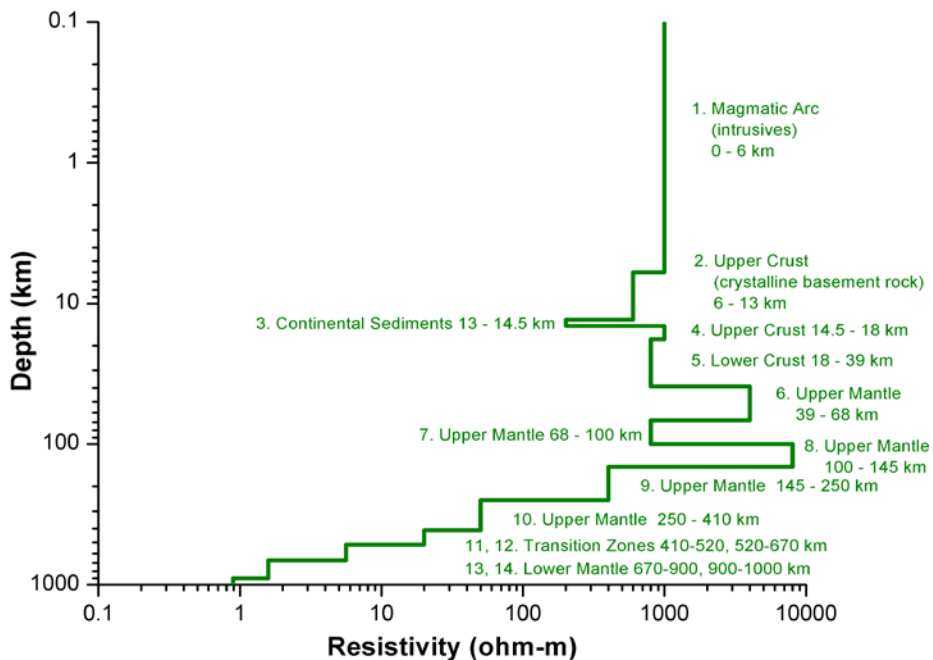
Preliminary earth conductivity models for IP-4 and PT-1 regions, provided by USGS, are shown in Figure 7 and Figure 8 respectively.

**Figure 7: IP-4 (Great Plains) 1-D Earth conductivity model [6]**



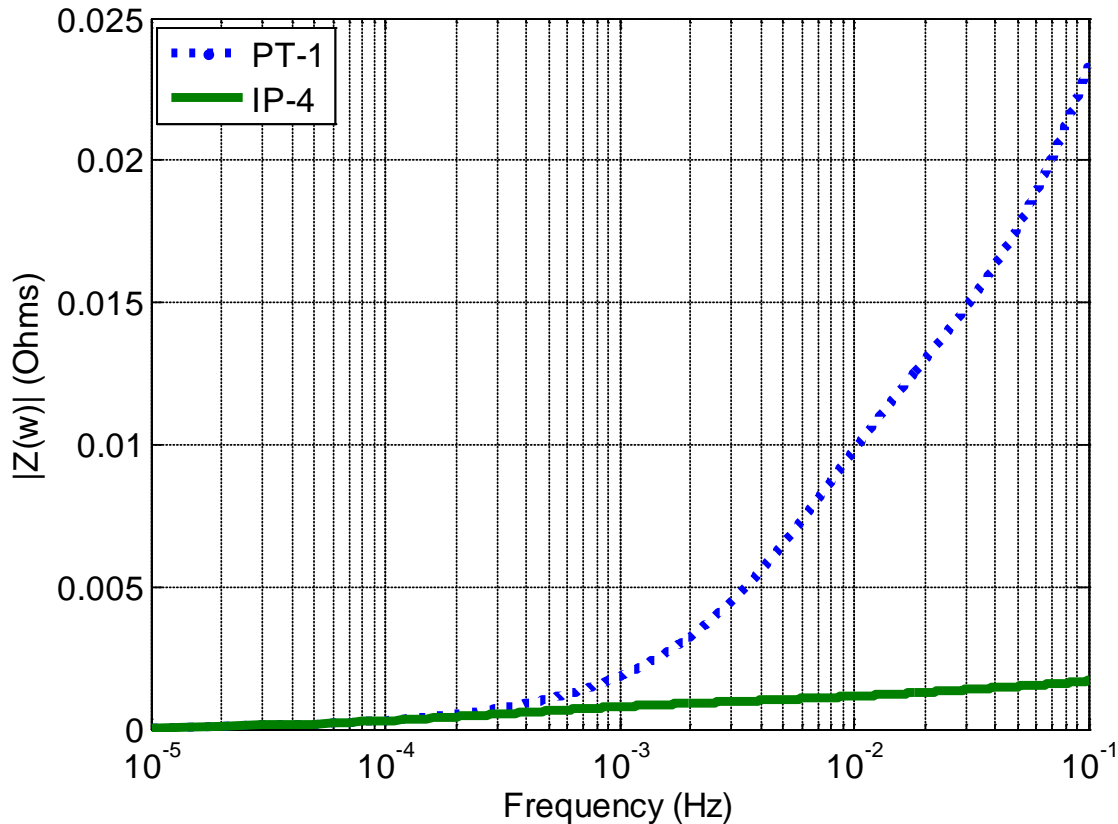
Resistivity values and depths have been interpreted from published geological reports and maps, and may differ from actual conditions measured by a geophysical survey and/or borehole.

**Figure 8: PT-1 (Piedmont) 1-D Earth conductivity model [6]**



The surface impedance for each of these models is shown in Figure 9 and was calculated using equations (5) to (8). The frequency response data provided in Figure 9 demonstrate the differences that can exist between various physiographic regions, and that these differences are frequency dependent.

**Figure 9: Frequency response of two layered Earth conductivity models.**



The frequency response (magnitude and phase) of the earth surface impedance can then be used with either measured or synthetic geomagnetic field data to calculate the induced geoelectric field. Example calculations made using the magnetic field data for March 13-14, 1989 are provided here. Data collected by magnetic observatories in the US are available from the USGS (<http://geomag.usgs.gov/>) and Canadian observatories from the GSC (<http://www.nrcan.gc.ca/geomag>) or through the INTERMAGNET web site (<http://www.intermagnet.org/>).

A Fast Fourier Transform (FFT) of the magnetic data from the Ottawa Magnetic Observatory gives the magnetic field spectrum shown in Figure 10a [7]. These spectral values are multiplied by the surface impedance values (see Figure 10b) which results in the geoelectric field spectrum shown in 10c. An inverse Fast Fourier Transform (IFFT) of this spectrum then gives the geoelectric field values in the time domain. These calculations are made using the eastward component of the geomagnetic field to determine the northward component of the geoelectric field (see (2)) and using the northward component of the magnetic field to give the eastward component of the geoelectric field (see (3)). The original geomagnetic field data and calculated geoelectric fields in the time domain are shown in Figure 11. The time series values of  $E_x$  and  $E_y$  can be used as inputs in subsequent GIC modeling and analysis.

**Figure 10: Frequency domain parameters in geoelectric field calculations [7].**  
 a) Geomagnetic field spectrum, b) Surface impedance, and c) Geoelectric field spectrum

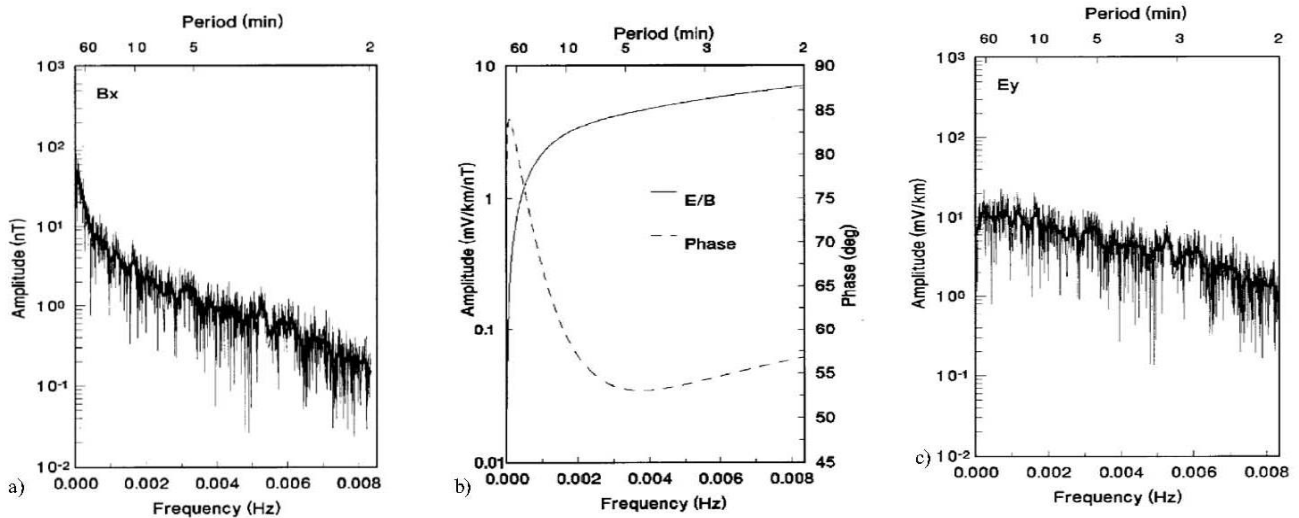
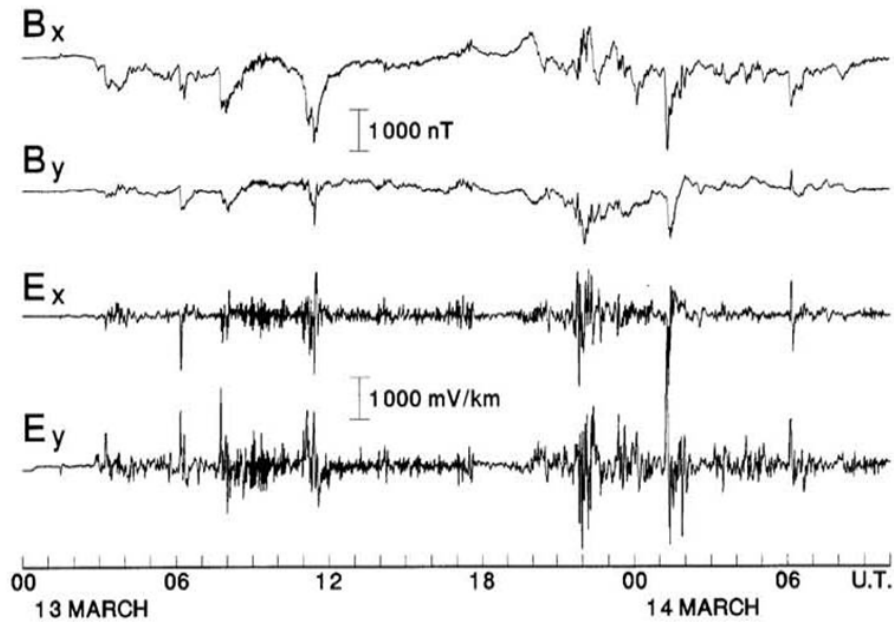


**Figure 11: Recordings from the Ottawa Magnetic Observatory and calculated geoelectric field for March 13-14, 1989 [7].**



In some situations, an extreme case (i.e., a 1-in-100 year) storm may be denoted by the estimated maximum geoelectric field magnitude. Depending upon the analysis being performed, this magnitude may be applied directly or used to scale historical measurement data.

Statistical analysis of geoelectric fields, calculated using geomagnetic field data from IMAGE stations located in Northern Europe, was applied in [8] to determine the range of geomagnetic storm intensities that might be expected to occur once in a 100 year period. This analysis indicates a 100-year peak geoelectric field of 5 V/km and 20 V/km for high and low conductive regions, respectively. These geoelectric field values were projected for



high latitude regions only, and considerable research continues to explore potential geomagnetic storm intensities for North America. However, an important outcome from the research presented in [8] is the effect of geomagnetic latitude on the resulting geoelectric fields. Research findings indicated that that the geoelectric field magnitudes may experience a dramatic drop across a boundary located at about 40-60 degrees of geomagnetic latitude.

The geomagnetic latitude for North America is shown in Figure 12. As shown, the inhabited regions of the U.S. and Canada span approximately 35 degrees of geomagnetic latitude (35 degrees to 70 degrees). Research by Pulkkinen, et al, indicates that the geoelectric field is highly dependent on the geomagnetic latitude [8] as indicated by the maximum geoelectric field magnitudes estimated assuming low earth conductivity, for two historical storms and plotted in Figure 13.

**Figure 12: Geomagnetic latitude of North America**

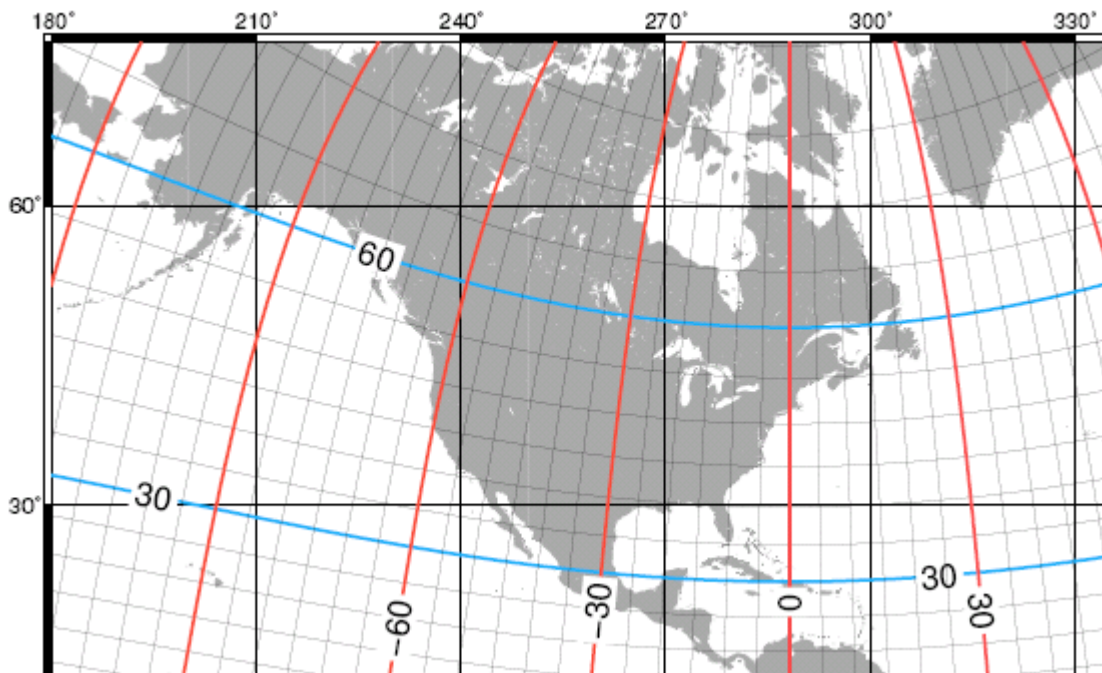
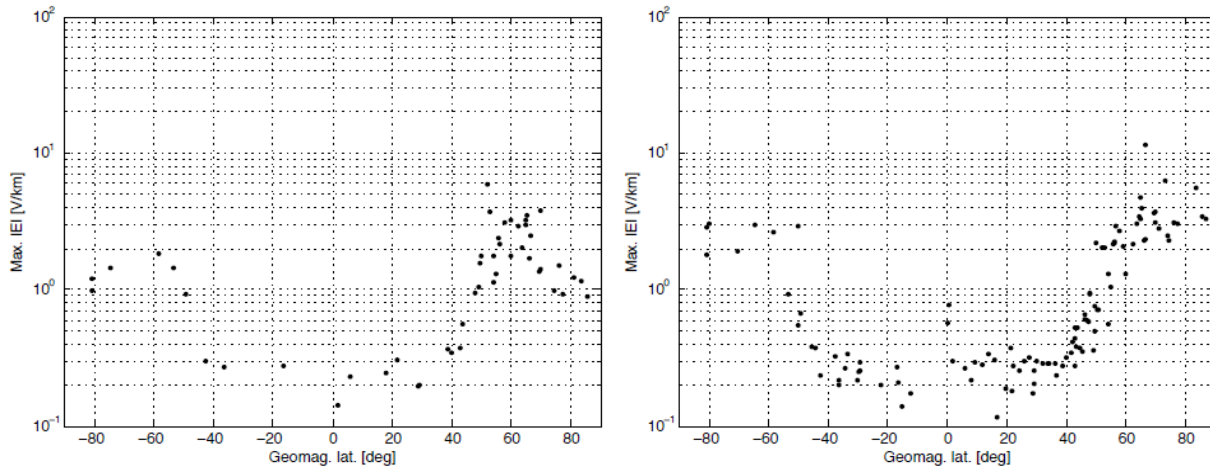


**Figure 13: Geomagnetic latitude distributions of the maximum computed geoelectric field**  
**a) March 13-15, 1989 b) October 29-31, 2003 [8].**



Relative scaling or correction factors that account for the influence of geomagnetic latitude on the estimated geoelectric field magnitude can be determined from the data presented in Figure 13, or using data from other events and earth conductivities. As shown in Figure 13, the estimated geoelectric field consistently portrays an order of magnitude and exponential drop between 40 and 60 degrees for both storms and in both hemispheres. A set of scaling factors which capture these observations is provided in Table 1.

**Table 1: Scaling Factors for 1-in-100 Year Storm**

Geomagnetic Latitude (Degrees)	Scaling Factor ( $\alpha$ )
$\leq 40$	0.100
41	0.112
42	0.126
43	0.141
44	0.158
45	0.178
46	0.200
47	0.224
48	0.251
49	0.282
50	0.316
51	0.355
52	0.398
53	0.447
54	0.501
55	0.562
56	0.631
57	0.708
58	0.794
59	0.891
$\geq 60$	1.000



The following procedure can be used to scale the geoelectric field values of a 1-in-100 year GMD event provided in [8] to account for general features of a specific region such as earth conductivity and geomagnetic latitude.

1. Select the 100-year storm magnitude of 5 V/km for regions with high earth conductivity or 20 V/km for regions assumed to have low earth conductivity.
2. Scale the 100-year geoelectric field magnitude to account for local geomagnetic latitude using the correction factors,  $\alpha_1$  provided in Table I using linear interpolation.

$$|E|_{corrected} = \alpha * |E|_{100-year} \tag{9}$$

3. For systems spanning several geographic and/or physiographic regions a weighted average or the largest projected value may be used as a conservative approach.

It should be noted that this is a general scaling factor and that geoelectric fields calculated with more specific earth conductivity information may actually be lower than those estimated in [8]. For instance [5] estimates that the geoelectric field in Quebec during the March 1989 event was in the order of 2 V/km as opposed to the 6 V/km value that could be gathered from Figure 13 (b). The cause of the two outlying data points, i.e. 6 V/km and 12 V/km shown in Figures 13(a) and 13(b), respectively, is a current research topic, and is not well understood by the scientific community at the time of publication of this report.

## Chapter 2 – Modeling GIC

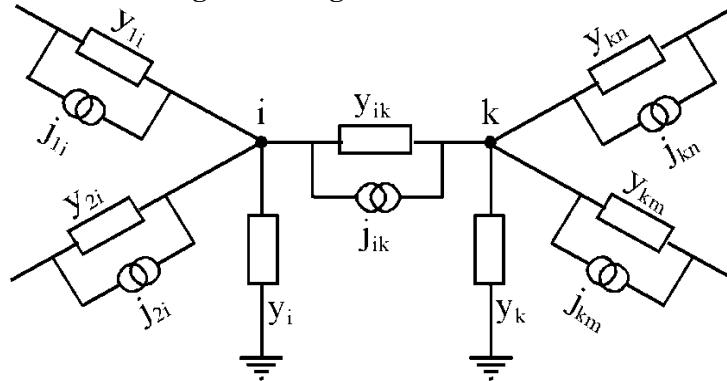
Because GIC are very low frequency, the ac network model is generally reduced to its dc equivalent [9]. The following sections describe the modeling theory and component models necessary for calculating GIC in a bulk power system.

### Theory

In the nodal admittance matrix method the power network is considered as nodes connected together and to ground. Driving voltages (emfs) are converted to equivalent current sources. For a voltage source  $e$  and impedance  $z$ , the corresponding equivalent circuit has components  $y = 1/z$  and  $j = e/z$ . A matrix solution is then obtained for the voltage of each node. The node voltages are then used to obtain the GIC in the network.

To develop the general equations for the nodal admittance matrix method consider nodes  $i$  and  $k$  in the middle of a network as shown in Figure 14. Here,  $y_{ik}$  represents the admittance of the transmission line between nodes  $i$  and  $k$  (note that  $y_{ik} = y_{ki}$ ), and  $y_i$  and  $y_k$  represent the admittances to ground from nodes  $i$  and  $k$  respectively.

**Figure 14: Modelling GIC using the nodal admittance matrix method**



Applying Kirchhoff's current law we can write an equation for any node  $i$  of the form

$$\sum_{k=1}^N i_{ki} = i_i \quad k \neq i \quad (10)$$

The current in a line is determined by the current source, the voltage difference between nodes at the ends of the line, and the admittance of the line

$$i_{ki} = j_{ki} + (v_k - v_i) y_{ki} \quad (11)$$

Substituting into (10) gives

$$\sum_{k=1}^N j_{ki} + \sum_{k=1}^N (v_k - v_i) y_{ki} = i_i \quad (12)$$

We make the further substitution

$$J_i = \sum_{k=1}^N j_{ki} \quad (13)$$

where  $J_i$  is the total of the equivalent source currents directed into each node. Thus we obtain the equation

$$J_i + \sum_{k=1}^N (v_k - v_i) y_{ki} = i_i \quad (14)$$

This equation involves the nodal voltages,  $v_i$ , and the current to ground from each node,  $i_i$  as unknowns. The nodal voltage  $v_i$  is related to the current to ground  $i_i$  by Ohm's law so we can substitute for either  $v_i$  or  $i_i$  to obtain equations involving only one set of unknowns. In this derivation we make the substitution

$$i_i = v_i y_i \quad (15)$$

Substituting for  $i_i$  gives equations involving only the node voltages  $v_i$  as the unknowns:

$$J_i + \sum_{k=1}^N (v_k - v_i) y_{ki} = v_i y_i \quad (16)$$

Regrouping terms gives

$$J_i = v_i y_i + \sum_{k=1}^N v_i y_{ki} - \sum_{k=1}^N v_k y_{ki} \quad (17)$$

This can be written in matrix form

$$[J] = [Y][V] \quad (18)$$

where the column matrix  $[V]$  contains the voltages  $v_k$  and  $[Y]$  is the admittance matrix in which the diagonal elements are the sums of the admittances of all paths connected to node  $i$ , and the off-diagonal elements are the negatives of the admittances between nodes  $i$  and  $k$ , i.e.

$$Y_{ii} = y_i + \sum_{k=1}^N y_{ki} \quad k \neq i \quad (19)$$

$$Y_{ki} = -y_{ki} \quad (20)$$

The voltages of the nodes are then found by taking the inverse of the admittance matrix and multiplying by the nodal current sources.

$$[V] = [Y]^{-1} [J] \quad (21)$$

These node voltages can be substituted into (11) to give the currents in the branches and into (15) to give the currents to ground from each node.

An important feature of the single-phase dc modeling technique described herein is that the resulting GIC flows are total “three-phase” quantities. For example, the GIC flow computed using (17) is the summation of all three phases. As such, the computed values must be divided by three if per-phase values are required. The same holds true for transformers. The exception is the GIC flow in the substation ground grid. In this case, the computed GIC is the actual GIC flow into the grid and does not require further modification.

Because of matrix sparsity, a direct solution of (21) is not practical for realistic bulk power systems due to the large number of buses involved. As a result, sparse matrix techniques such as those presented in [10] and [11] are generally used to simplify the computation.

An example GIC calculation of a theoretical six bus power system is provided in Appendix B.

### Time Series Calculations

Although future improvements are to be expected, currently most analyses – performed using commercially available tools – assume a uniform geoelectric field and apply the steady state calculation approach. In the steady-state approach, a geoelectric field value is assumed and used as input to the GIC model. However, there are situations where time series GIC data are required, for example thermal analysis of transformers. A convenient procedure for scaling the results of either the steady-state method, in particular computing GIC flows for various geoelectric fields, or for creating time series GIC data follows.

GIC is computed for a 1 V/km Eastward geoelectric field (Northward component is assumed zero) and again for a 1 V/km Northward geoelectric field (Eastward component is assumed zero). The results of these two calculations can then be scaled using any arbitrary geoelectric field provided that the geoelectric field is laterally uniform in the geographic region under consideration [12]. The scaling function is described in (22)

$$GIC_{new} = |E| \{ GIC_E \sin \theta + GIC_N \cos \theta \} \quad (22)$$

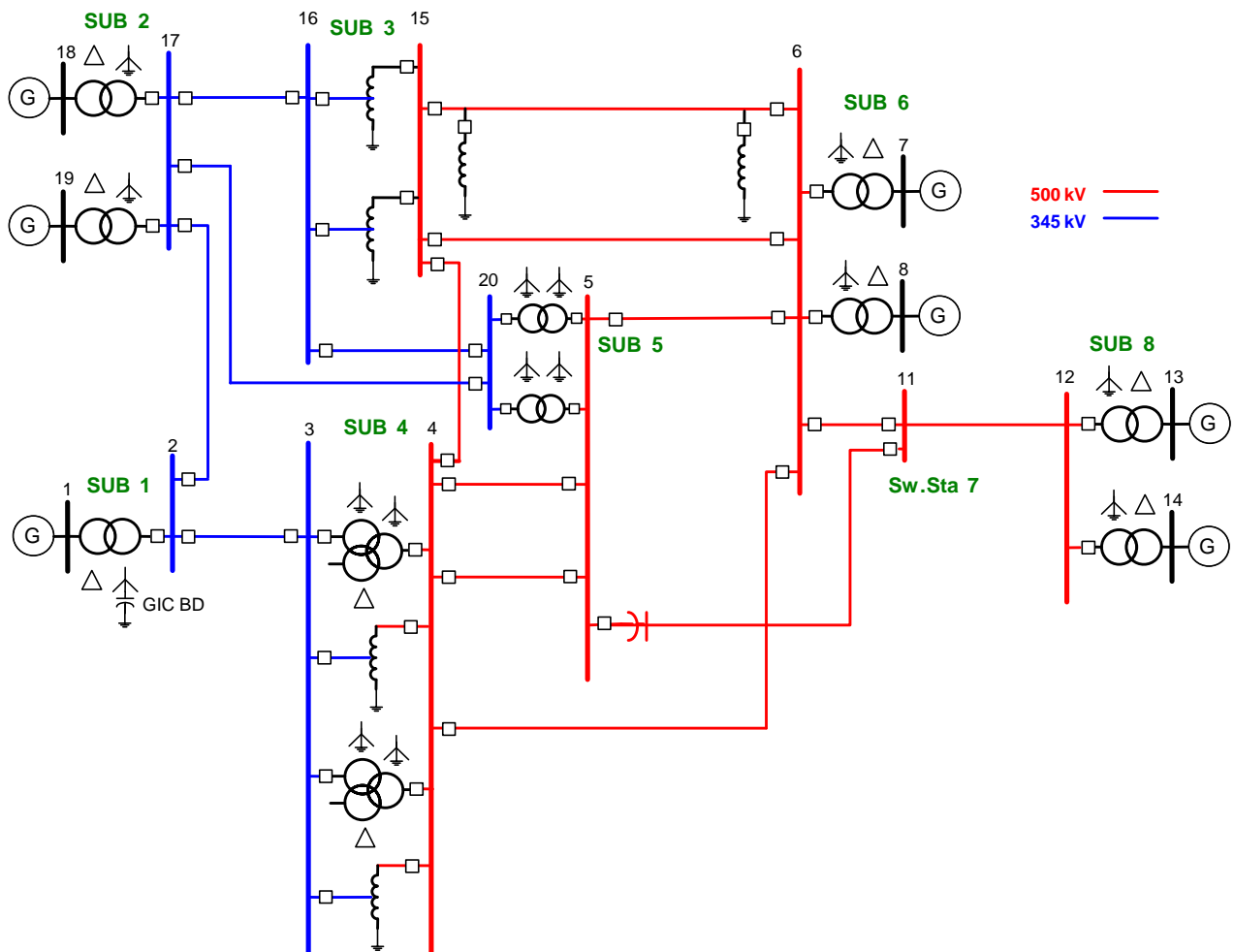
where  $GIC_{new}$  is the new value of GIC (amps),  $|E|$  is the magnitude of the arbitrary geoelectric field (V/km),  $\theta$  is the angle of the geoelectric field vector (radians),  $GIC_E$  is the GIC due to a 1 V/km Eastward geoelectric field (amps), and  $GIC_N$  is the GIC due to a 1 V/km Northward geoelectric field (amps). Time series geoelectric field data in concert with (22) can be used to construct time series GIC flows needed for transformer thermal models or other such analyses.

## Practical Details

### Introduction

One of the first steps in calculating GIC in a bulk power system is to develop a dc equivalent model of the system. These models are normally assembled using a combination of information from: 1) ac models used to perform power flow analysis or short circuit studies, 2) available equipment resistance data, and 3) geographic information for the substations. The example system provided in **Figure 15** shows many of the various system components which require dc models. Such components include: transformers, transmission lines, shunt reactors, series capacitor, substation ground grids, and GIC blocking devices. Generators can be excluded from the analysis because they are isolated at dc from the rest of the transmission system; thus, an equivalent dc model is not required. Additional modeling details that are normally not a part of the ac model, but which are required to assemble the dc model include: geographic locations of the substations (latitude/longitude), equivalent substation ground grid resistance (including the effects of overhead shield wires and other ground current paths) and dc winding resistance of transformers and shunt devices (e.g. shunt reactors). The following sections describe methods for developing a dc model of each of the components represented in **Figure 15**.

**Figure 15: Single-line diagram of example power system used to demonstrate the various components that require dc models**



The dc model data required for the individual network components are summarized in Table 2. Additional details for each component are covered in subsequent sections of this chapter. There can be significant difference between the desired model data and an estimated value (based on a next best alternative) which can lead to inaccurate representation of GIC distribution in some modeled network branches. To assure best accuracy and the data consistency needed for sharing model data with other study engineers, estimated values should only be used when the desired resistive data is not obtainable.

**Table 2: Summary of network component and associated resistive data for a one-phase GIC network model**

Network Component	Most Appropriate Data For Accurate Modeling	Best Alternative Estimate - When Desired Model Data Is Not Available	Data Sources and Comments
Grounded wye winding of conventional transformer	Measured dc resistance of the winding at nominal tap and adjusted to 75 °C and divided by 3 (see note)	50% of the total per-unit copper loss resistance converted to actual ohms at winding base values and divided by 3	dc resistance and copper loss resistance are obtained from transformer test records. Transformer copper loss resistance from power flow model data base.
Autotransformer series windings	Measured dc resistance of each winding at nominal tap and adjusted to 75 °C and divided by 3 (see note)	50% of the total per-unit copper loss resistance converted to actual ohms at full winding base values and divided by 3	dc resistance and copper loss resistance are obtained from transformer test records. Transformer copper loss resistance from power flow model data base.
Autotransformer common winding	Measured dc resistance of each winding at nominal tap and adjusted to 75 °C and divided by 3 (see note)	50% of the total per-unit copper loss resistance converted to actual ohms at $V_H$ winding base values and divided by $(V_H/V_X - 1)^2$ and divided by 3	dc resistance and copper loss resistance are obtained from transformer test records. Transformer copper loss resistance from power flow model data base.
Shunt reactor	Measured dc resistance of winding adjusted to 75 °C and divided by 3 (see note)	Measured ac copper loss resistance of winding at factory test temperature and divided by 3	dc resistance and copper loss resistance are obtained from test records.
Ground grid to remote earth including the effects of overhead shield wires	Measured value from ground grid test	Calculated value from design modeling	Commissioning or routine grounding integrity test data, or ground grid design software.
Neutral blocking device	Nameplate ohms for a resistor; 100 $\mu\Omega$ for solid ground modeled as a resistor; 1 M $\Omega$ for capacitor (modeled as a resistance)	Not applicable	Depends on capability of network modeling software, but the study tool must be able to handle this branch as closed, open, or fixed value of resistance.

Transmission line	One third of the individual phase dc resistance adjusted to 50 °C	One third of the individual phase ac resistance adjusted to 50 °C or 75 °C	Conductor manufacturer tables, system electrical design data, network model data for power flow and fault studies.
Series line capacitor	100 μΩ for bypassed state modeled as a resistor; 1 MΩ for inserted state modeled as a resistor	Not applicable	Depends on capability of network modeling software, but the study tool must be able to handle this branch in either its short circuit (bypassed) or capacitive (inserted) state.

Note: Winding resistance data provided in transformer test reports may represent the total resistance of the three phases combined, and must be divided by 3 to obtain the resistance of a single winding.

**Transformers**

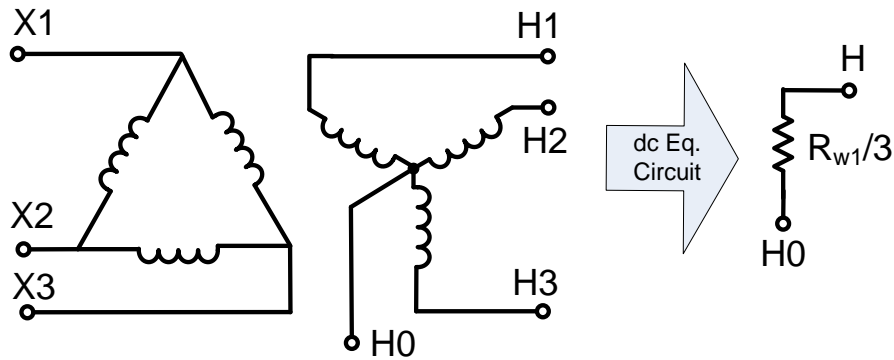
Power transformers are represented by their dc equivalent circuits, i.e. mutual coupling between windings and windings without physical connection to ground are excluded. An exception to this, as described later, is the series winding of an autotransformer which is always included in the model. Dc models are generally used for the purposes of computing GIC; however, time-domain models which replicate the behaviour of the transformer over a wide band of frequencies (including dc) can be constructed. For brevity, only dc models will be discussed here.

Important note: Resistance values used for modeling transformers in the dc network are best obtained from transformer test reports. If these data are not readily available then the dc resistance of the transformer windings may be estimated using positive sequence resistance data contained in power flow and short circuit models. However, it should be stressed that estimated values may contain considerable error. An evaluation performed by the NERC GMD TF on a select number of transformers indicated that the magnitude of error between estimated resistance values and those provided in transformer test reports can be on the order of 35% or higher. Thus, estimated values should only be used in situations when dc winding resistances are unavailable.

***Generator Step-Up Transformers***

The dc equivalent circuit of a delta grounded-wye generator step-up unit (GSU) is provided in Figure 16. Note that the delta winding is not included in the dc equivalent because it does not provide a steady-state path for GIC flow. The HO terminal refers to the neutral point that is ordinarily connected directly to the substation ground grid model (neutral bus shown in Figure 19). If GIC mitigation equipment is employed, the impedance of the GIC blocking device would be inserted between the HO terminal and the equivalent ground resistance of the station.

Figure 16: Single-Phase dc equivalent circuit of a GSU



$R_{w1}$  in

Figure 16 is defined as the dc resistance of the grounded-wye winding. The dc resistance of the grounded-wye winding may be estimated using positive sequence resistance data. The per-unit positive sequence resistance,  $R_{HX}$ , includes both the resistance of the high-voltage winding (Ohms),  $R_H$ , and the referred value of the low voltage winding (Ohms),  $R_X$ , as indicated in (23),

$$R_{HX} = \frac{R_H + n^2 R_X}{Z_{bh}} \quad (23)$$

where  $Z_{bh}$  refers to the base impedance (Ohms) on the high-voltage side of the transformer and  $n$  is the transformer turns ratio ( $V_H/V_X$ ). The assumption is made that the high-voltage winding resistance and the referred value of the low-voltage winding are approximately equal [9] and [13]; thus, the resistance of the high voltage winding can be estimated using (24)

$$R_H = \frac{1}{2} \cdot R_{HX} \cdot Z_{bh} \quad (24)$$

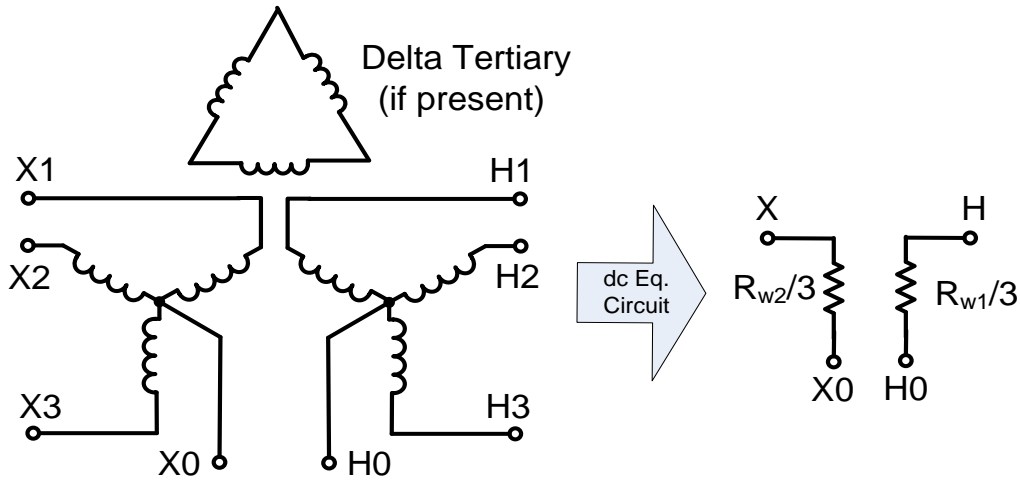
Skin effect and changes in the resistance as a function of winding operating temperature are usually ignored.

### ***Two-Winding and Three-Winding Transformers***

The dc equivalent circuit of both a two-winding and three-winding transformer is provided in Figure 17. Note the delta tertiary winding (if applicable) is not included in the model since it does not provide a path for GIC to flow in steady-state. Both winding neutral nodes (i.e. X0 and H0) are modeled explicitly. In some cases, either the X0 or H0 terminal may be ungrounded. The neutral terminal of grounded wye windings (e.g. X0 or H0) is ordinarily connected directly to the substation ground grid model (neutral bus shown in Figure 19) or left floating depending on the application. If GIC mitigation equipment is employed, the impedance of the GIC blocking device would be inserted between the H0 and/or X0 terminals and the equivalent ground resistance of the station. Ungrounded wye windings are excluded in GIC calculations because they do not provide a path for GIC flow.



**Figure 17: Single-phase dc equivalent circuit of a two-winding or three-winding transformer**



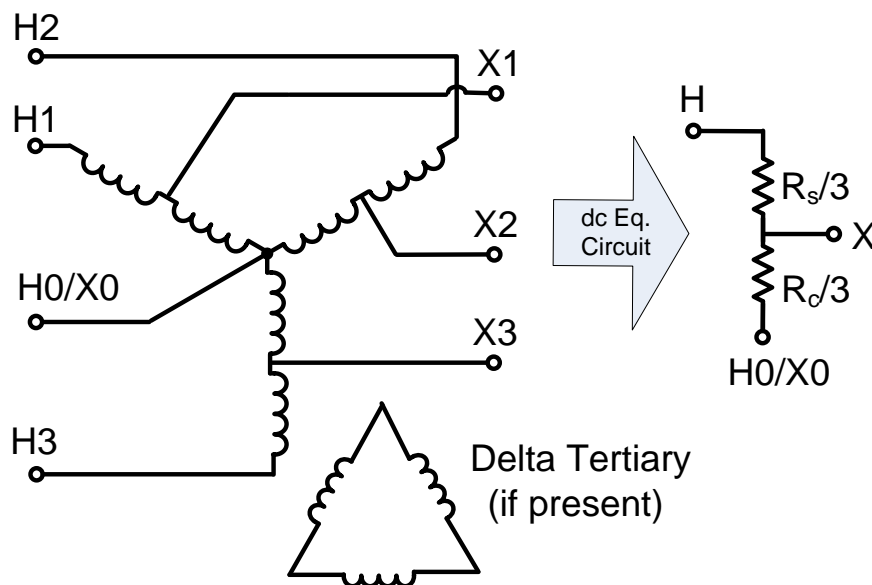
$R_{w1}$  and  $R_{w2}$  in Figure 17 refer to the dc winding resistance values of the high voltage or extra-high voltage and medium voltage windings, respectively. If test report data are not available then the dc winding resistances may be estimated using the same procedure described for GSUs.

**Autotransformers**

The dc equivalent circuit of an autotransformer is provided in Figure 18.

Note that the delta tertiary winding (if present) is not included in the model because it does not provide a steady-state path for GIC flow. The common autotransformer neutral terminal (H0/X0) is modeled explicitly, and is ordinarily connected directly to the substation ground grid model (neutral bus shown in Figure 19). If necessary to model GIC mitigation equipment, the impedance of the device would be inserted between the H0 terminal and the equivalent ground resistance of the station.

**Figure 18: Single-phase dc equivalent circuit of a two-winding or three-winding autotransformer**



$R_s$  and  $R_c$  are defined as the dc resistance of the series and common windings, respectively. The dc resistance of the series and common windings can be estimated using (10) and (11), where  $R_{HX}$  is the per-unit positive sequence resistance, and  $n = V_H/V_X$  or the ratio of the line-to-ground voltages of the H and X terminals.

$$R_s = \frac{I}{2} \cdot R_{HX} \cdot Z_{bh} \quad (25)$$

$$R_c = \frac{I}{2} \cdot \frac{R_{HX} \cdot Z_{bh}}{(n-1)^2} \quad (26)$$

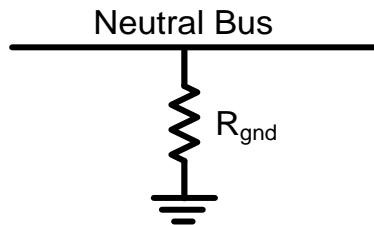
### Substation Ground Grid and Neutral Connected GIC Blocking Devices

The equivalent resistance of the substation ground grid (including the effects of any transmission line overhead shield wires and/or distribution multi-grounded neutral conductors if applicable) to remote earth must be included in the model. The fundamental frequency ac resistance is typically used because it is approximately equivalent to the dc resistance. Note there is only a single substation ground resistance value for each substation; thus, it is connected to a common “neutral” bus, in the network model, as depicted in

Figure 19, where  $R_{gnd}$  is the resistance to remote earth of the substation ground grid. The number of connections to the neutral bus shown in

Figure 19 is determined by the number of grounded-wye transformer windings located in the substation.

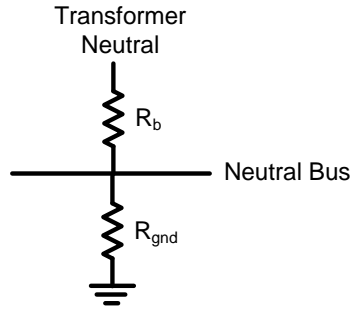
**Figure 19: Electrical model of substation ground grid to remote earth for use in GIC calculations**



The electrical model of a GIC blocking device is depicted in

Figure 20, where  $R_b$  is the resistance of the GIC blocking device. For study purposes, this network branch element must be capable of representing three possible states: solidly grounded; resistive grounded; and capacitive grounded. The three states can be modeled effectively as a resistor using a different resistance value for each possible state of the branch element. For example, a direct connection to ground would be represented as  $R_b = 0.1 \text{ m}\Omega$ , a blocking device represented by  $R_b = 1.0 \text{ M}\Omega$ , and a neutral resistor (if employed) would be represented by its specified resistance.

**Figure 20: Electrical model of GIC blocking device between transformer neutral and substation ground grid as used in GIC calculations**



Depending on the type of modeling software that is used, the model presented in

Figure 20 may be used in all cases with the difference being the value used for  $R_b$  to represent the various grounding arrangements. This enables accuracy without exceeding program computational limits associated with the numbers zero and infinity. A capacitive GIC blocking device presents very high impedance to GIC; thus, it can be modeled as a high resistance (e.g. 1.0 M $\Omega$ ), whereas, a solid ground is modeled as low resistance (e.g. 100  $\mu\Omega$ ). The actual resistance is used for a resistive blocking device.

### Transmission Line Models

Changes in magnetic field density,  $B$ , with respect to time result in an induced electric field as explained in Chapter 1. The driver of GIC is the geoelectric field (the electric field at the surface of the earth) integrated along the length of each transmission line which can be represented by a dc voltage source:

$$V_{dc} = \oint \vec{E} \circ d\vec{l} \quad (27)$$

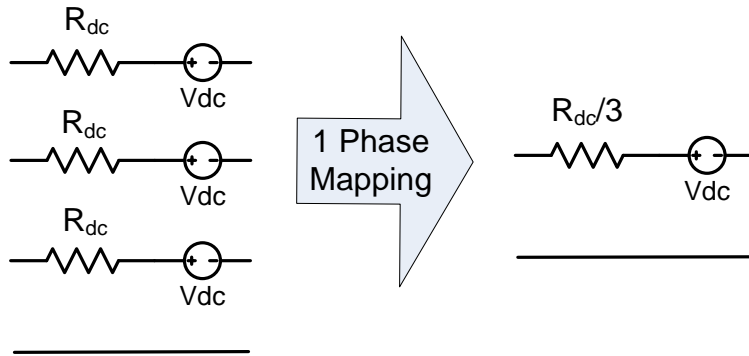
where,  $\vec{E}$  is the geoelectric field at the location of the transmission line, and  $d\vec{l}$  is the incremental line segment length including direction. If the geoelectric field is assumed uniform in the geographical area of the transmission line, then only the coordinates of the end points of the line are important, regardless of routing twists and turns. The resulting incremental length vector  $d\vec{l}$ , becomes  $\vec{L}$ . Both  $\vec{E}$  and  $\vec{L}$  can be resolved into their  $x$  and  $y$  coordinates. Thus, (27) can be approximated by (28)

$$\vec{E} \circ \vec{L} = E_x L_x + E_y L_y \quad (28)$$

where,  $E_x$  and  $E_y$  are the northward and eastward geoelectric fields (V/m), respectively, and  $L_x$  and  $L_y$  are the northward and eastward distances (m), respectively. If the geoelectric field is non-uniform, then (27) must be used. To obtain accurate values for the distance between substations (and to be consistent with substation latitudes and longitudes obtained from GPS measurements) it is necessary to take into account the non-spherical shape of the earth [14]. The earth is an ellipsoid with a smaller radius at the pole than at the equator. The precise values depend of the earth model used. The WGS84 model which is used in the GPS system is recommended. See Appendix A for details on computing  $L_x$  and  $L_y$ .

The dc equivalent circuit of a transmission line is depicted in Figure 21.

**Figure 21: Three-phase transmission line model and its single-phase equivalent used to perform GIC calculations**



$V_{dc}$  refers to the induced voltage computed using (27) or (28) and  $R_{dc}$  corresponds to the  $dc$  resistance of the phase conductors including the effects of conductor bundling if applicable.

The resistive data from ac power flow and fault studies is useable for modeling line resistance in GIC studies. Although it is preferred to use the  $dc$  resistance ( $R_{dc}$ ) of the transmission line, it is acceptable to use the ac resistance ( $R_{ac}$ ) value in most cases. The difference between  $R_{dc}$  and  $R_{ac}$  at 50 °C is less than 5% for conductors up to 1.25 inch in diameter, and less than 10% up to 1.5 inch diameter conductor. Conductor sizes beyond 1.5 inches in diameter should be evaluated for possible impact to model accuracy as the difference between ac and  $dc$  resistance could be significant for long transmission lines.

Although there is minimal difference between  $R_{dc}$  and  $R_{ac}$  at the same temperature, there is a considerable difference between resistance at ambient temperature and the values typically used in power flow studies. The resistance of a transmission conductor will be 10 to 15% higher at 50 °C than at 20 °C. Although less conservative, modeling with resistance at 50 °C is preferred because a loaded system is more susceptible to adverse impact under GIC conditions and the most stressful condition to study

Shield wires are not included explicitly as a GIC source in the transmission line model [15]. Shield wire conductive paths that connect to the station ground grid are accounted for in ground grid to remote earth resistance measurements and become part of that branch resistance in the network model.

### Blocking GIC in a Line

Series capacitors are used in the bulk power system to re-direct power flow and improve system stability. Series capacitors present very high impedance to the flow of GIC. This effect can be included in the model in a number of ways, one of which is by adding a very large resistance (e.g. 1 M $\Omega$ ) in series with the nominal  $dc$  resistance of the line (see  $R_{dc}$  in Figure 21) or removing the line from the model completely. Additional modeling complications arise when lines are segmented to accommodate the effects of non-uniform geoelectric fields, and special care must be taken to ensure numerical stability.

### Shunt Devices

The bulk power system generally uses two types of shunt elements to help control system voltage: shunt capacitors and shunt reactors. Shunt capacitors present very high impedance to the flow of GIC, and are consequently excluded in the  $dc$  analysis. Shunt reactors connected directly to the substation bus or transmission lines, on the other hand, can provide a low impedance path for GIC and should be included in the analysis. The  $dc$  model of a grounded-wye shunt reactor is the same as that of a grounded-wye winding of a GSU. If  $dc$  winding resistance values are unknown, they can be estimated using an assumed X/R ratio. Note that X/R ratio of a typical dead-tank shunt reactor can be far greater than the X/R ratio of a typical transformer of the same MVA rating. It is not uncommon for the X/R ratio of large shunt reactors to exceed 1000.

## Chapter 3 – Modeling Refinements

The preceding calculation methods use two particular assumptions in order to simplify the calculations: 1) the magnetic field variations are uniform over the area of the power system and 2) the earth conductivity structure only varies with depth (i.e., there are no lateral variations in conductivity). To improve the accuracy of the calculated geoelectric fields both the structure of the source magnetic field and the lateral variations in conductivity should be considered.

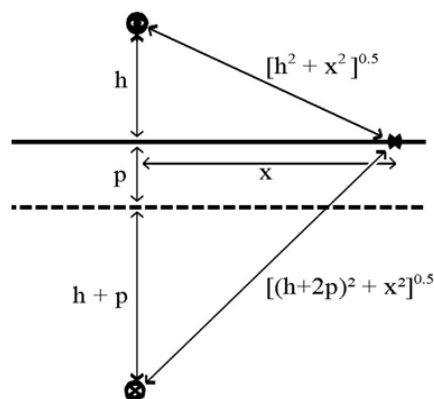
### Non-Uniform Source Fields

Various near-space electric current systems can generate magnetic field fluctuations anywhere on the ground. The spatial structure of the source field is highly dependent on the type of the source: for example magnetopause currents, tail current, ring current and auroral currents, all have distinct spatial signatures. Further, different sources dominate at different latitudes. However, magnetic field-aligned currents bring large amounts of near-space current down into the high-latitude ionosphere at about 100 km above the surface of the earth with amplitudes of millions of amperes [16]. These ionospheric currents are known as auroral currents or electrojets. The electrojet model is a crude approximation for the source of the geomagnetic field, but can be used as a basis for computing GIC and understanding GMD phenomenon in general.

As an example of non-uniform source fields, consider the auroral electrojet which is the cause of magnetic substorms that are responsible for the largest GIC in power systems. The magnetic and geoelectric fields produced by the auroral electrojet can be calculated using the complex image method [17]. First formulas are presented for the assumption that the electrojet can be considered as a line current at a height of 100 km. Then it is shown how the complex image method can be extended to include the width of the electrojet.

Figure 22 shows a line current at a height  $h$  above the earth's surface. The total variation fields at the earth's surface are due, as mentioned earlier, to the field of the external source plus the field due to the currents induced in the earth. However, it has been shown that the "internal" fields are approximated, to good accuracy, by the fields due to an image current at a complex depth. This means that the complex skin depth,  $p$ , can be represented as a reflecting surface so that the image current is the same distance below this level as the source current is above (Figure 22). The magnetic and geoelectric fields are then given by the source and image currents and their distances from the location on the surface as shown in Figure 22.

**Figure 22: Distances to an external line current at a height,  $h$ , and an image current at a complex depth  $h+2p$  from a location on the earth's surface.**



The magnetic and geoelectric fields at horizontal distance,  $x$ , from the source current are then given by

$$B_x = \frac{\mu_0 I}{2\pi} \left( \frac{h}{h^2 + x^2} + \frac{h + 2p}{(h + 2p)^2 + x^2} \right) \quad (29)$$

$$B_z = -\frac{\mu_0 I}{2\pi} \left( \frac{x}{h^2 + x^2} - \frac{x}{(h + 2p)^2 + x^2} \right) \quad (30)$$

$$E_y = -\frac{j\omega\mu_0 I}{2\pi} \ln \left[ \frac{\sqrt{(h + 2p)^2 + x^2}}{\sqrt{h^2 + x^2}} \right] \quad (31)$$

Where the complex skin depth is related to the surface impedance by the expression

$$p = \frac{Z_s}{j\omega\mu_0} \quad (32)$$

In practice, the auroral electrojet spreads over about six degrees of geomagnetic latitude. The current profile is difficult to determine but the studies that have been made shows that it can vary considerably. In practice, without special studies for each event, we cannot specify the current profile of the electrojet. However, a simple way to include the width of the auroral electrojet is to assume that the current has a Cauchy distribution. It can be shown that the fields produced by this current profile with a half-width  $a$  at a height  $h$  are the same as the fields produced by a line current at a height  $h+a$  [18]. The expressions for the magnetic and geoelectric fields at the earth's surface in this case are

$$B_x = \frac{\mu_0 I}{2\pi} \left( \frac{h + a}{(h + a)^2 + x^2} + \frac{h + a + 2p}{(h + a + 2p)^2 + x^2} \right) \quad (33)$$

$$B_z = -\frac{\mu_0 I}{2\pi} \left( \frac{x}{(h + a)^2 + x^2} - \frac{x}{(h + a + 2p)^2 + x^2} \right) \quad (34)$$

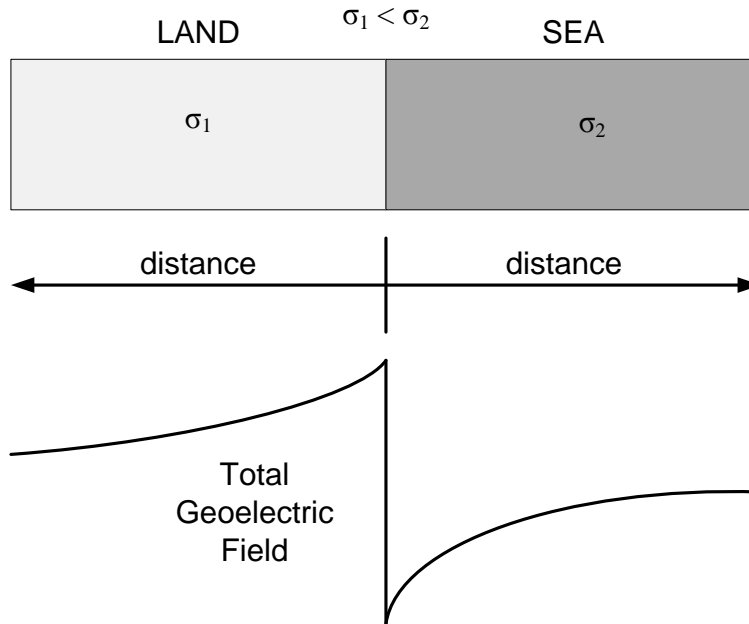
$$E_y = -\frac{j\omega\mu_0 I}{2\pi} \ln \left[ \frac{\sqrt{(h + a + 2p)^2 + x^2}}{\sqrt{(h + a)^2 + x^2}} \right] \quad (35)$$

These geoelectric fields can be used as input into a power system model to calculate the GIC that would be produced by an electrojet at a specified location relative to the power system.

## Non-Uniform Earth Structure

Another factor affecting the geoelectric field is conductivity boundaries, such as at a coast line or different geological regions within the power network under study [7]. The horizontal conductivity structure at the interface of a land/sea boundary (i.e. coastline), is characterized by a sharp change as depicted in Figure 23.

**Figure 23: Geoelectric fields perpendicular to coastline**



The higher conductivity of the sea in relation to the land means that higher electric currents are induced in the sea as compared with the land. When these currents are directed perpendicular to the coast there is a difference in the current density “arriving” at the coast from the sea compared to that “departing” from the coast into the land. Because charge cannot accumulate at the boundary, this condition gives rise to a potential gradient that acts to decrease the current in the sea and increase the current in the land so as to achieve current continuity at the boundary. Thus on the landward side of the boundary the geoelectric field perpendicular to the boundary is larger than would be expected from simply considering the land conductivity alone [7]. The size of the increased geoelectric field and how far it extends inland depend on the conductivity of the area, the depth of the sea and the characteristics of the geomagnetic field [7]. A method for investigating the coastal effect on geoelectric fields and GIC calculations can be found in [19].

## Including Neighboring Systems

GIC can flow in or out of the network from/to adjacent networks and in most cases accurate modeling at system boundaries requires including the effects of neighboring systems. Unless the complete neighboring system (and its neighbors) is to be included in the GIC modeling, it is necessary to represent the adjacent system by an equivalent circuit.

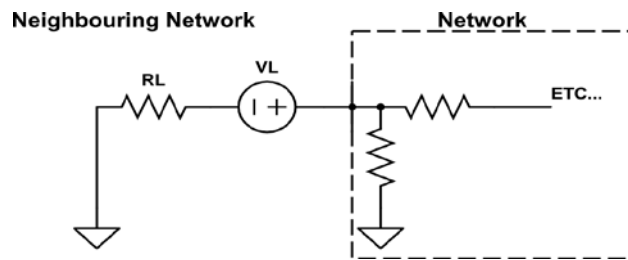
Determining accurate equivalent networks in GIC calculations is an ongoing research topic; however, to date, there are at least three methods that can be used to represent the neighboring system:

1. Ignore the neighboring network and leave the connection as an open circuit. This is the simplest method and requires the least amount of information from the neighboring grid.

2. Represent the neighboring network as the line to the first substation and its resistance to ground.
3. Represent the neighboring network as a very long line. For situations, as commonly occurs, where the line resistance is much greater than the resistance to ground through the substation,  $R_L \gg R_S$ , it can be shown that this leads to an equivalent circuit with  $V_{th} = V_L$  and **Error! Bookmark not defined.**  $R_{th} = R_L$  as shown in Figure 24.

The most accurate choice of the equivalent circuits is the third model, i.e. representing the Thevenin equivalent as a line voltage and line resistance as shown in Figure 24. Ignoring the neighboring network gives the greatest calculation error [20].

**Figure 24: Thevenin equivalent circuit for a neighboring network determined from the resistance and induced voltage in the first transmission line**



The discussion above relates specifically to the treatment of neighboring areas for GIC flow analysis within the study area. Studies of GIC-related effects, such as ac voltage depression or harmonics require that the neighboring systems present reasonable boundary conditions to the area or system where detailed study is desired. To achieve these boundary conditions, it is typically necessary for the GIC flow through transformers within some extent of the neighboring systems to also be reasonably accurate. Thus, the area of GIC flow study must generally be wider in extent than the system where these effects are to be evaluated. Simulation results provided in [20] show that modeling four buses into the neighboring network yield results that are indistinguishable from those obtained using the full network model.



## References

---

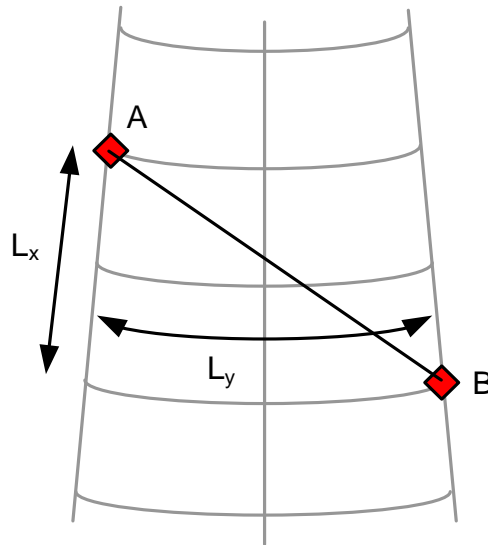
1. Juan A. Martinez-Velasco, *Power System Transients: Parameter Determination*, CRC Press, 2010.
2. Fiona Simpson, Karsten Bahr, *Practical Magnetotellurics*, Cambridge University Press, 2005.
3. L. Trichtchenko, D. H. Boteler, "Modeling of Geomagnetic Induction in Pipelines", *Annales Geophysicae*, 2002, 20: 1063-1072.
4. J. L. Gilbert, W. A. Radasky, E. B. Savage, "A Technique for Calculating the Currents Induced by Geomagnetic Storms on Large High Voltage Power Grids", *IEEE International Symposium on Electromagnetic Compatibility (EMC)*, Aug. 2012, pp. 323-328.
5. L. Marti, A. Rezaei-Zare, D. Boteler, "Calculation of Induced Electric Field during a Geomagnetic Storm using Recursive Convolution", *IEEE Transactions on Power Delivery*, 2013.
6. One-Dimensional Earth Resistivity Models for Selected Areas of Continental United States & Alaska, EPRI 1026430, Dec. 2012.
7. D. H. Boteler, "Geomagnetically Induced Currents: Present Knowledge and Future Research", *IEEE Transactions on Power Delivery*, Vol. 9, No. 1, January 1994, pp. 50-58.
8. Pulkkinen, E. Bernabeu, J. Eichner, C. Beggan, and A. W. P. Thompson, "Generation of 100-year geomagnetically induced current scenarios," *Space Weather*, vol. doi:10.1029/2011SW000750, 2012.
9. Investigation of Geomagnetically Induced Currents in the Proposed Winnipeg-Duluth-Twin Cities 500 kV Transmission Line, EPRI EL-1949, July 1981.
10. W. F. Tinney, V. Brandwajn, S. M. Chan, "Sparse Vector Methods", *IEEE Transactions on Power Apparatus and Systems*, Vol. PAS-104, Feb. 1985, pp. 295-301.
11. T. Overbye, T. Hutchins, J. Weber, S. Dahman, "Integration of Geomagnetic Disturbance Modeling into the Power Flow: A Methodology for Large-Scale System Studies", North American Power Symposium 2012, September 9-11, University of Illinois at Urbana-Champaign.
12. D. H. Boteler, Q. Bui-Van, J. Lemay, "Directional Sensitivity to Geomagnetically Induced Currents of the Hydro-Quebec 735 kV Power System", *IEEE Transactions on Power Delivery*, Vol. 9, No. 4, October 1994, pp. 1963-1971.
13. *Westinghouse Electrical Transmission and Distribution Reference Book*, ABB Power Systems, Inc., 1964.
14. R. Horton, D. H. Boteler, T. J. Overbye, R. J. Pirjola, R. Dugan, "A Test Case for the Calculation of Geomagnetically Induced Currents", *IEEE Transactions on Power Delivery*, Vol. 27, Issue: 4, October, 2012, pp.2368-2373.
15. R. Pirjola, "Calculation of geomagnetically induced currents (GIC) in a high-voltage electric power transmission system and estimation of effects of overhead shield wires on GIC modelling," *Journal of Atmospheric and Solar-Terrestrial Physics*, vol. 69, pp. 1305-1311, 2007.

16. Space Weather 101, EPRI 1025860, November 2012.
17. D.H. Boteler, and R. J. Pirjola, "The complex image method for calculating the magnetic and electric fields produced at the surface of the earth by the auroral electrojet," *Geophys. J. Int.*, 132, 31-40, 1998.
18. D.H. Boteler, R. J. Pirjola, and L. Trichtchenko, "On calculating the magnetic and electric fields produced at the earth's surface by a 'wide' electrojet," *J. Atmos. Solar Terr. Phys.*, 62, 1311-1315, 2000.
19. R. Pirjola, "Practical Model Applicable to Investigating the Coast Effect on the Geoelectric Field in Connection with Studies of Geomagnetically Induced Currents", *Advances in Applied Physics*, Vol. 1, 2013, No. 1, pp. 9-28.
20. D. H. Boteler, A. J. C. Lackey, L. Marti, S. Shelemy, "Equivalent Circuits for Modelling Geomagnetically Induced Currents from a Neighbouring Network," Paper 002195, Proceedings IEEE Power & Energy Society General Meeting, Vancouver, 21-25 July 2013.

## Appendix I – Calculating Distance Between Substations

Consider a transmission line between substations A and B as shown in Fig A.1. Assuming a spherical earth, the NS distance is simply calculated from the difference in latitude of substations A and B. However, there is no similar simple relationship for the EW distance because, as shown in Fig A.1, lines of longitude converge as they approach the pole. Consequently it is necessary to take into account the latitude of the substations when converting their longitudinal separation into a distance.

Figure A.1. Substation Location Coordinates



To get more accurate values (and to be consistent with substation latitudes and longitudes obtained from GPS measurements) it is necessary to take into account the non-spherical shape of the earth. The earth is an ellipsoid with a smaller radius at the pole than at the equator. The precise values depend of the earth model used. Here we use the WGS84 model (Table A.1) which is used in the GPS system.

Table A.1 Parameters of the WGS84 Earth Model

Parameter	Symbol	Value
Equatorial radius	a	6378.137 km
Polar radius	b	6356.752 km
Eccentricity squared	$e^2$	0.00669437999014

The North-South distance is given by:

$$L_N = \frac{\pi}{180} M \cdot \Delta lat \quad (A.1)$$

where,  $M$  is the radius of curvature in the meridian plane and is described by (A.2)

$$M = \frac{a(1 - e^2)}{(1 - e^2 \sin^2 \phi)^{1.5}} \quad (A.2)$$

Substituting in the values from Table A.1. gives the expression for the Northward distance in km:

$$L_N = (111.133 - 0.56 \cos(2\phi)) \cdot \Delta lat \quad (A.3)$$

where,  $\Delta lat$  is the difference in latitude (degrees) between the two substations A and B, and  $\phi$  is defined in (A.4) as the average of the two latitudes:

$$\phi = \frac{LatA + LatB}{2} \quad (A.4).$$

Similarly the East-West distance is given by:

$$L_E = \frac{\pi}{180} N \cos \phi \cdot \Delta long \quad (A.5),$$

where  $N$  is the radius of curvature in the plane parallel to the latitude as defined in (A.6) and  $\Delta long$  is the difference in longitude (degrees) between the two substations A and B

$$N = \frac{a}{\sqrt{1 - e^2 \sin^2 \phi}} \quad (A.6).$$

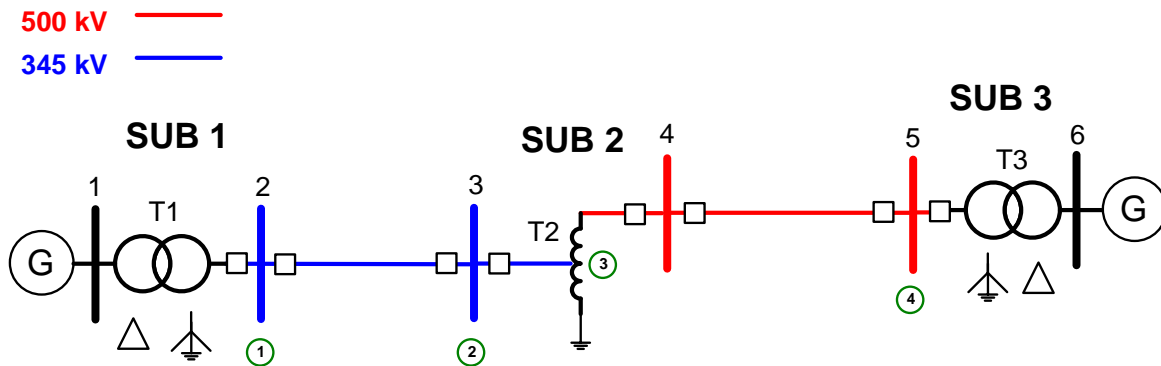
Substituting the values from Table A.1 gives the following expression for the Eastward distance in km.

$$L_E = (111.5065 - 0.1872 \cos 2\phi) \cdot \cos \phi \cdot \Delta long \quad (A.7).$$

## Appendix II – Example of GIC Calculations

The following section describes the steps that can be taken to compute GIC flow in a power system. The example six-bus system that will be analyzed is shown in Figure B-1. Bus numbers are shown at bus locations. Encircled numbers refer to circuit nodes that will be used later in the calculation of GIC.

Figure B-1: Example system used to compute GIC



Required system data are provided in Tables B-1 through B-3.

Table B-1: Substation location and ground grid resistance

Name	Latitude	Longitude	Grounding Resistance (Ohms)
Sub 1	33.613499	-87.373673	0.2
Sub 2	34.310437	-86.365765	0.2
Sub 3	33.955058	-84.679354	0.2

Table B-2: Transmission line information

Line	From Bus	To Bus	Length (km)	Resistance (Ohms/phase)
1	2	3	121.03	3.525
2	4	5	160.18	4.665

Table B-3: Transformer and autotransformer winding resistance values

Name	Resistance W1 (ohm/phase)	Resistance W2 (ohm/phase)
T1	0.5	N/A
T2	0.2 (series)	0.2 (common)
T3	0.5	N/A

For these calculations we use the geomagnetic coordinate system with x axis in the northward direction, y axis in the eastward direction, and z axis vertically downward. The procedure described in Appendix A can be used to compute northward and eastward distances and are shown in Table B-4.

**Table B-4: Eastward and northward distance calculation results**

Line	From Bus	To Bus	Northward Distance (km)	Eastward Distance (km)
1	2	3	-77.499	-92.96
2	4	5	39.518	-155.22

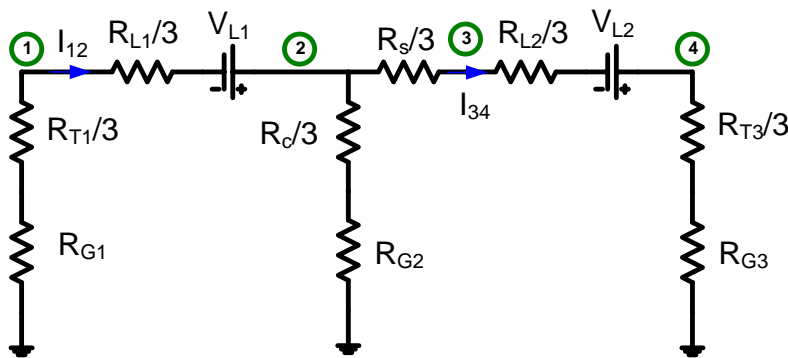
Assuming an electric field magnitude of 10 V/km with Eastward direction, the resulting induced voltages were computed using (28) and found to be as shown in Table B-5.

**Table B-5: Induced voltage calculation results**

Line	From Bus	To Bus	Induced Voltage (Volts)
1	2	3	-929.6
2	4	5	-1552.3

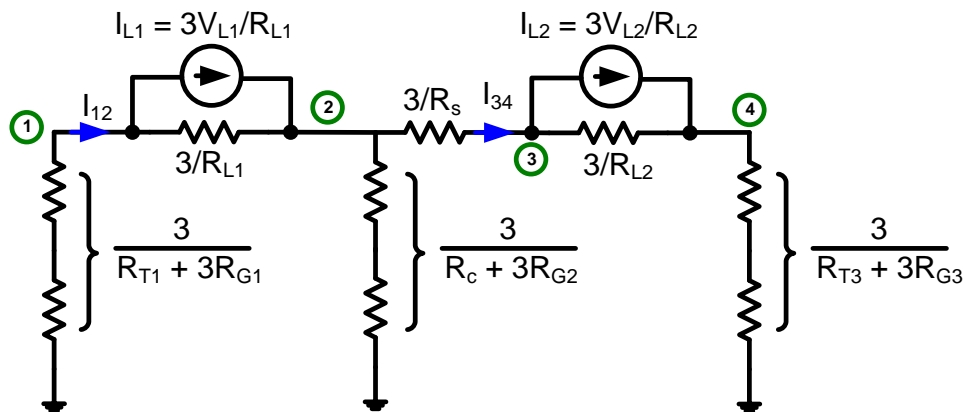
The next step is to construct an equivalent circuit of the system. An equivalent circuit of the system shown in Figure B-1 is provided in Figure B-2. Note the node names correspond to the locations indicated in Figure B-1.

**Figure B-2: Equivalent circuit of example system**



Although the equivalent circuit shown in Figure B-2 can be solved directly, it is more convenient to perform the calculations using nodal analysis where the voltage sources are converted to current sources, and all impedance elements are converted to their equivalent admittances. The resulting equivalent circuit is shown in Figure B-3.

**Figure B-3: Equivalent circuit of example system in nodal form**



The admittance matrix of the circuit shown in Figure B-3 can be readily constructed, and is shown in general form in (B.1):

$$Y = \begin{bmatrix} \frac{3}{R_{T1}+3R_{G1}} + \frac{3}{R_{L1}} & -\frac{3}{R_{L1}} & 0 & 0 \\ -\frac{3}{R_{L1}} & \frac{3}{R_s} + \frac{3}{R_{L1}} + \frac{3}{R_c+3R_{G2}} & -\frac{3}{R_s} & 0 \\ 0 & -\frac{3}{R_s} & \frac{3}{R_s} + \frac{3}{R_{L2}} & -\frac{3}{R_{L2}} \\ 0 & 0 & -\frac{3}{R_{L2}} & \frac{3}{R_{L2}} + \frac{3}{R_{T3}+3R_{G3}} \end{bmatrix} \quad (B.1)$$

Substituting the appropriate values into (B.1) results in (B.2):

$$Y = \begin{bmatrix} 3.578 & -0.851 & 0 & 0 \\ -0.851 & 19.601 & -15 & 0 \\ 0 & -15 & 15.643 & -0.643 \\ 0 & 0 & -0.643 & 3.37 \end{bmatrix} mhos \quad (B.2)$$

The resulting nodal current injections were found to be:

$$I_{L1} = \frac{3V_{L1}}{R_{L1}} = -791.15 \text{ amps} \quad I_{L2} = \frac{3V_{L2}}{R_{L2}} = -998.23 \text{ amps}$$

The current vector can be constructed using the nodal currents as shown in (B.3):

$$I = \begin{bmatrix} -I_{L1} \\ I_{L1} \\ -I_{L2} \\ I_{L2} \end{bmatrix} \quad (B.3)$$

The resulting node voltages are computed using Ohms Law

$$V = [Y]^{-1}I = \begin{bmatrix} 229.72 \\ 36.25 \\ 87.08 \\ -279.56 \end{bmatrix} \quad (B.4)$$

The GIC flows (all three phases combined) are computed using various relationships derived from the circuit. The results are as follows:

$$I_{T1} = V_1 \left( \frac{3}{R_{T1}+3R_{G1}} \right) = 626.5 \text{ amps} \quad (B.5);$$

$$I_{12} = I_{L1} + (V_1 - V_2) \frac{3}{R_{L1}} = -626.5 \text{ amps} \quad (B.6);$$

$$I_s = (V_2 - V_3) \frac{3}{R_s} = -762.45 \text{ amps} \quad (B.7);$$

$$I_c = V_2 \left( \frac{3}{R_c+3R_{G2}} \right) = 135.95 \text{ amps} \quad (B.8);$$

$$I_{34} = I_{L2} + (V_3 - V_4) \frac{3}{R_{L2}} = -762.45 \text{ amps} \quad (B.9);$$

$$I_{T3} = V_4 \left( \frac{3}{R_{T3}+3R_{G3}} \right) = -762.45 \text{ amps} \quad (B.10).$$

The per-phase GIC values can be determined from the results provided in (B.5)-(B.10) by dividing by 3.

Similar calculations were performed with varying orientations of the electric field. A neutral blocking device was also considered in the neutral of the autotransformer by setting the corresponding substation ground grid resistance to a very large value (1MΩ). The results of these calculations are provided in Tables B-6 and B-7. The per-phase GIC values can be determined from the results provided in Tables B-6 and B-7 by dividing the values shown by 3.

**Table B-6: Results without neutral blocking device**

<b> E  (V/km)</b>	<b>Orientation (degrees)</b>	<b>I<sub>T1</sub> (amps)</b>	<b>I<sub>12</sub> (amps)</b>	<b>I<sub>s</sub> (amps)</b>	<b>I<sub>c</sub> (amps)</b>	<b>I<sub>34</sub> (amps)</b>	<b>I<sub>T3</sub> (amps)</b>
10	0	409.87	-409.87	126.78	-536.65	126.78	126.78
10	30	668.21	-668.21	-271.43	-396.78	-271.43	-271.43
10	60	747.50	-747.50	-596.91	-150.59	-596.91	-596.91
10	90	626.50	-626.50	-762.45	135.95	-762.45	-762.45
10	120	337.63	-337.63	-723.69	386.06	-723.69	-723.69
10	150	-41.71	41.71	-491.02	532.73	-491.02	-491.02
10	180	-409.87	409.87	-126.78	536.65	-126.78	-126.78

**Table B-7: Results with neutral blocking device installed in the neutral of the autotransformer**

<b> E  (V/km)</b>	<b>Orientation (degrees)</b>	<b>I<sub>T1</sub> (amps)</b>	<b>I<sub>12</sub> (amps)</b>	<b>I<sub>s</sub> (amps)</b>	<b>I<sub>c</sub> (amps)</b>	<b>I<sub>34</sub> (amps)</b>	<b>I<sub>T3</sub> (amps)</b>
10	0	-107.60	107.60	107.59	0.00	107.59	107.59
10	30	-444.72	444.72	444.72	0.00	444.72	444.72
10	60	-662.68	662.68	662.68	0.00	662.68	662.68
10	90	-703.07	703.07	703.07	0.00	703.07	703.07
10	120	-555.08	555.08	555.08	0.00	555.08	555.08
10	150	-258.35	258.35	258.36	0.00	258.36	258.36
10	180	107.60	-107.60	-107.59	0.00	-107.59	-107.59



## Appendix III – NERC GMD Task Force Leadership Roster

Position	Name and Title	Company	Contact Info
Chair	Kenneth Donohoo, P.E. Director, System Planning	Oncor Electric Delivery 2233 B Mountain Creek Parkway Dallas, TX 75211	214.743.6823 kenneth.donohoo@oncor.com
Vice Chair	Frank Koza, P.E. Executive Director of Infrastructure Planning	PJM Interconnection, LLC 955 Jefferson Ave Norristown, PA 19403	610.666.4228 kozaf@pjm.com
Team Leader Equipment Model Development and Validation	Luis Marti, Ph.D., PE Manager, Professional Development and Special Studies	Hydro One Networks 483 Bay Street TCT15N Toronto, ON M5G 2P5	416.345.5317 luis.marti@ HydroOne.com
Team Leader GIC Model Development and Validation	Randy Horton, Ph.D., P.E. Chief Engineer, Transmission Technical Support	Southern Company Services 42 Inverness Parkway Birmingham, AL 35242	205.257.6352 jrhorton@southernco.com
Team Leader System Operating Practices, Tools, and Training	Frank Koza, P.E. Executive Director of Infrastructure Planning	PJM Interconnection, LLC 955 Jefferson Ave Norristown, PA 19403	610.666.4228 kozaf@pjm.com
Technical Support Electric Power Research Institute	Richard Lordan Technology Director	EPRI 3420 Hillview Avenue Palo Alto, CA 94304	650.855.2435 rilordan@epri.com
Technical Support Electric Power Research Institute	Jason Taylor Project Manager	EPRI 942 Corridor Park Blvd Knoxville, TN 37932	865.218.8077 jtaylor@epri.com
NERC Staff Coordinator	Noha Abdel-Karim, Ph.D. Senior Engineer, Reliability Assessment	NERC 3353 Peachtree Rd NE, Suite 600 Atlanta, GA 30326	404.446-4699 noha.karim@nerc.net
NERC Staff Coordinator	Mark Olson Standards Developer	NERC 3353 Peachtree Rd NE, Suite 600 Atlanta, GA 30326	404.446.9760 mark.olson@nerc.net